Scientific paper

Meso-scale Modeling of Anomalous Moisture Transport in Concrete Considering Microstructural Change of Cement-based Material

Puttipong SRIMOOK[1*], Keigo OGAWA[2], Ippei MARUYAMA[3,4]
[1]Researcher, Department of Architecture, Graduate School of Engineering, The University of Tokyo, Tokyo, Japan.
[2]Master student, Department of Architecture, Graduate School of Engineering, The University of Tokyo, Tokyo, Japan.
[3]Professor, Department of Urban Environment, Graduate School of Environmental Studies, Nagoya University, Nagoya, Japan.
[4]Professor, Graduate School of Engineering, Department of Architecture, Graduate School of Engineering, The University of Tokyo, Tokyo, Japan.
*Corresponding author, *E-mail (Italic)*: srimook-puttiipong@bme.arch.t.u-tokyo.ac.jp

Abstract
Moisture transport is the key phenomenon indicating the deterioration of the durability and structural performance of concrete structures. Although various studies have attempted to evaluate moisture transport in concrete, an anomalous behavior, which does not follow the root-t law compared to other porous material, was not explicitly taken into account. To quantitatively evaluate anomalous moisture transport, this study developed a couple of numerical methods between the truss-network model (TNM) and the rigid-body-spring model (RBSM) for this purpose. The colloidal behavior of calcium-silicate-hydrate (C-S-H), which is the major phase of cement-based material, was introduced to consider the anomalous behavior and mechanical response regarding the microstructural change of cement paste as well as cracks that significantly accelerate the moisture transport in concrete. The numerical results indicated that both microstructural change of cement paste and rapid absorption through cracks cause anomalous behavior. In addition, the numerical results suggest that volumetric change of cement paste should rely on water content related to the colloidal behavior of C-S-H in order to reproduce the realistic expansion and the closure of cracks during a rewetting process that affects structural performance and durability of concrete.
Keywords: Anomalous moisture transport, Microstructural change, Concrete, C-S-H, Cracks

1. Introduction
Moisture transport in concrete has been highlighted as the key phenomena that indicate the deterioration of structural performance and durability of RC structures. In term of structural performances, various studies clarified the impact of moisture content on mechanical properties of concrete such as compressive strength, tensile strength, Young's modulus, etc. (Pihlajavaara, 1974; Sereda et al., 1966; Wittmann, 1968; Yurtdas et al., 2004b, 2004a, 2006, 2015) and structural performance of RC members (e.g., initial stiffness, strength, natural frequency, etc.) (Maruyama, 2016, 2022; Nakarai et al., 2016; Sasano et al., 2018; Sasano & Maruyama, 2019; Sato & Kawakane, 2008; Satya et al., 2021; Tanimura et al., 2007). In terms of durability, moisture evaporation cause drying-shrinkage cracks in concrete, which have been clarified as the accelerator for mass transport such as moisture (Van Belleghem et al., 2016; K. Wang et al., 1997; Yang et al., 2006; P. Zhang et al., 2010, 2017), chloride (Aldea et al., 1999; Asselin et al., 2023; Rodriguez & Hooton, 2003), carbon dioxide (De. Schutter, 1999), and radioactive substances (Yamada et al., 2019) that could lead to the severe damage for concrete.

Regarding the aforementioned influence of moisture content, it is necessary to quantitatively evaluate the moisture transport in concrete. However, the moisture transport in concrete is not as simple as other porous materials because anomalous behavior has been reported. Therefore, the quantitative evaluation of moisture transport and mechanical response in cement-based material (CBM) could not be reproduced based on the traditional approach. In the traditional concept, concrete was considered a rigid porous material. Thus, the moisture transport characteristics were evaluated based on the root-t law, which is the basis of various theories elucidating the linear relationship of moisture transport characteristics with the square root of time such as Fick's law of diffusion (Paul et al., 2014), Lucas-Washburn equation for the dynamics of capillary flow (Washburn, 1921). However, Hall et al. (1995) reported anomalous capillary liquid water absorption in the cementitious material. The moisture characteristics (e.g., penetration depth and absorbed water amount) in CBM follow the root-t law at the initial stage, however, the slower sorption process was observed at the later stage.

The similar anomalous behavior was confirmed by the latter studies that investigated the moisture transport in the unsaturated CBM (Hall, 2007; Kiran et al., 2021; Lockington & Parlange, 2003; Martys & Ferraris, 1997; Saeidpour & Wadsö, 2015; Taylor et al., 1999; Zhou et al., 2017). Recently, studies based on neutron magnetic resonance (NMR) were conducted to investigate the microstructure of CBM. Regarding the NMR studies on capillary water absorption of CBM (Fischer et al., 2015; Gajewicz et al., 2016), NMR data reported that water redistribution in the pore system occurs due to the water movement in the calcium-silicate-hydrate (C-S-H) structure. Because C-S-H is the main component of CBM that shows the colloidal behavior according to the strong dependence on its surrounding water molecules (Jennings, 2000, 2008; Jennings et al., 2008; Setzer, 2009; Thomas & Jennings, 2006), the microstructural change of cement paste (MCCP) regarding the colloidal behavior of C-S-H was accentuated as the cause of the anomalous behavior.

Several modeling approaches have been proposed to clarify or simplify anomalous moisture transport in CBM such as the effect of moisture content (Rucker-Gramm & Beddoe, 2010), multi-phasic moisture transport (Z. Zhang & Angst, 2020), and the fourth root of time law (Villagrán Zaccardi et al., 2017). Nevertheless, the aforementioned numerical methods did not reflect the origins of the anomaly. Although the fourth root of time law was proposed to consider the MCCP regarding the pore refinement due to internal swelling, it could not explicitly reproduce the influence of MCCP on anomalous behavior. The latter studies based on neutron magnetic resonance (NMR) proposed the dynamic microstructural change model that could explicitly introduce the colloidal behavior of C-S-H for moisture transport. Nevertheless, our previous study on dried mortar (Srimook & Maruyama, 2023b) found that the dynamic microstructural model considering the influence of MCCP is insufficient to reproduce the moisture distribution and liquid water uptake characteristics. This is because microcracks occurred during the pre-drying process causing the rapid absorption through cracks at the surface area. Therefore, it is essential to introduce MCCP and microcracks in order to explicitly introduce anomalous moisture transport in concrete.

From our previous studies, the modeling of moisture transport in cracked concrete was proposed based on a couple of numerical methods, a Rigid-Body Spring Model (RBSM) and a Truss-Network Model (TNM), that could easily couple the mechanical behavior (e.g., volumetric change, cracking) and mass transport (moisture transport), respectively. The anomaly regarding MCCP was introduced in the TNM based on the dynamic microstructural change model (Janota et al., 2022; McDonald et al., 2020) and the rapid absorption through cracks was explicitly modeled based on microcracks in concrete reproduced by the RBSM. The numerical investigation on liquid water uptake in pre-dried concrete was conducted and validated based on an experiment in our research group. The numerical results indicated that our modeling approach could consider the influence of microstructural change and cracks on anomalous liquid water uptake. Furthermore, the concrete expansion-induced closure of cracks, which indicated the impact of liquid water uptake on structural performance, was reported.

In this study, the anomalous moisture transport in cracked concrete was further investigated. The numerical models for the anomalous moisture transport and volumetric change were revised for the realistic phenomena. Aggregates were assumed as a non-absorbance material (no pores), thus, the moisture transport and volumetric change of aggregate were excluded to accentuate the influence of the cement-based material expansion that caused the microcracks and their closure during the drying and rewetting, respectively. Regarding the study on the microstructure of cement-based material (Maruyama et al., 2019; Maruyama, Nishioka, et al., 2014; Maruyama, Sasano, et al., 2014), various evidence indicated the mechanical behavior of concrete significantly related to MCCP, which is also caused by the colloidal behavior of C-S-H. Therefore, the volumetric change model was revised to determine based on water related to the C-S-H structure (interlayer and gel water) instead of the total water in the pore system. The modeling approach was validated based on the current experimental results. A further numerical investigation was conducted to discuss the mechanism of anomalous moisture transport and the influence of MCCP on volumetric change. The purpose is to clarify their importance for reproducing anomalous moisture transport and mechanical responses. In addition, the mortar expansion-induced closure of cracks, which might have a significant impact on structural performance and durability, was further investigated to clarify the mechanism.

2. Numerical method

This study aims to numerically investigate the anomalous liquid water uptake in cracked concrete. Therefore, the couple numerical method between the rigid-body-spring-model (RBSM) and truss-network model (TNM), which has the potential to couple the moisture transport and mechanical response such as volumetric change, cracking behavior (Sasano & Maruyama, 2021), must be implemented. In this section, the concept of the RBSM and TNM was elucidated. The numerical models considering the anomalous moisture transport, moisture transport through cracks, volumetric change of mortar, and related phenomena (e.g., mesoscale constitutive model, mechanical property change, time-dependent microcrack (TDM) model) were described in the following section.

2.1 Rigid-body-spring-model (RBSM) and truss-network model (TNM)

The RBSM is the discrete approach-based numerical method, which was proposed and further developed to easily deal with the mechanical behavior of concrete and the strong discontinuity behavior of brittle material like cracking behavior (Bolander & Saito, 1998; Kawai, 1978; Saito & Hikosaka, 1999; Yamamoto et al., 2008). **Figure** 1 (Upper right) is the schematic diagram elucidating the concept of RBSM. The concrete was discretized into an assemblage of rigid particles based on the Voronoi diagram. Each particle was interconnected with the set of zero-size springs (one of normal spring and two of shear springs) at the integral point, which was determined based on the two vertices and gravity center of the boundary surface. Based on an assemblage of Voronoi elements, the deformation (volumetric change) was reproduced by the global stiffness, which was constructed by the stiffness of zero-size springs and the assumed spring length (the distance between the barycenter of adjacent Voronoi elements). At the force equilibrium, the normal spring bears the compressive and tensile stress perpendicular to the interface, whereas two shear springs are orthogonal and bear the shear stress parallel to the interface. The moment (torsional and rotational) borne at the interface of each particle was automatically accounted for from the deformation of normal springs at several integral points. The deformation and crack width were interpreted from the strain of the zero-size spring at the equilibrium and the assumed spring length.

The TNM is a simplified one-dimensional finite element method (FEM) that was continuously developed to reproduce the mass transport in concrete and couple with the RBSM for reproducing the volumetric change due to several phenomena (Bolander & Berton, 2004; Nakamura et al., 2006). **Fig**. 1 (lower right) shows the schematic diagram of TNM. The TNM is a network of truss elements embedded in Voronoi elements and each truss element was considered a linear conduit for the potential flow. The truss elements generated between the Voronoi nuclei, and the intermediate point of the boundary surface are internal truss elements (blue line) that act as the linear conduit with a cross-section area Voronoi surface. To avoid the redundancy of truss volume, the calibration factor, a ratio of all truss element volume to the total volume of the specimen, is introduced. The truss elements generated between the intermediate point, and the middle point of the line between the vertex are boundary truss elements (green line) that act as the linear conduit with a cross-section area determined by the crack displacement at the integral point. The boundary truss elements are activated with respect to the presence of cracks.

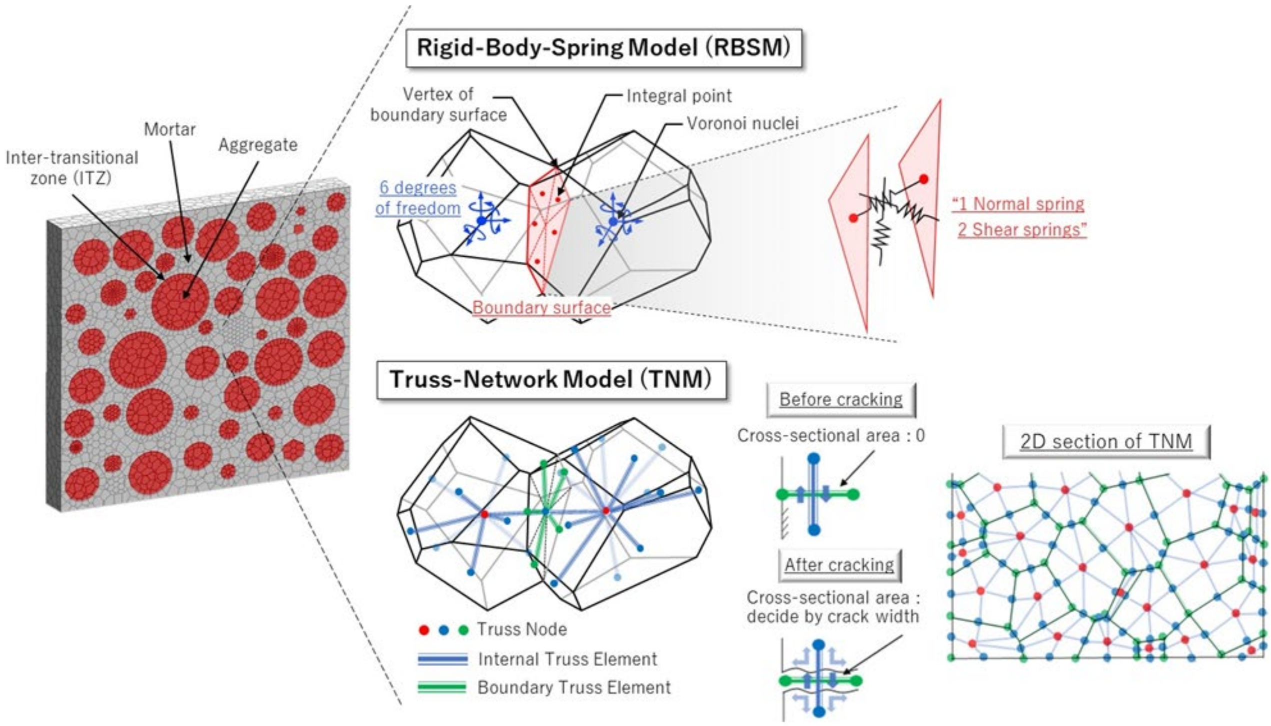

Fig. 1. Schematic diagram of rigid-body-spring model (RBSM) and truss-network model (TNM) (Nakamura et al., 2006; Srimook & Maruyama, 2023a; Yamamoto et al., 2008, 2014).

2.2 Constitutive models of springs for mesoscale RBSM

In RBSM, the nonlinear behavior was introduced into the springs by constitutive laws in order to reproduce the deformation, stress, and fracture behavior. Because this study accentuates the mesoscale, the constitutive models of spring in RBSM were employed to represent the nonlinear behavior of mortar, aggregate, and inter-transitional zone (ITZ).

For the mortar and aggregate, the constitutive models developed for concrete (Sasano & Maruyama, 2019; Yamamoto et al., 2008) were employed to represent the nonlinear behavior under tension and compression for a normal spring and shear behavior for shear springs. For ITZ, it was considered as the weak zone owing to higher porosity (Diamond & Huang, 2001; Scrivener et al., 2004), lower strength (Monteiro & Andrade, 1987; Zimbelmann, 1985), fracture energy (Rao & Prasad, 2011), and Young modulus (Jebli et al., 2018; Xie et al., 2015) compared to the bulk cement or mortar. Therefore, the constitutive models, which were developed to represent the characteristics of ITZ (Sasano & Maruyama, 2021), were introduced for normal and shear springs at the interface between mortar and aggregate. The tensile behavior was modeled based on the same constitutive models of concrete, but the reduction factor (α) was introduced to consider the weakness of the ITZ. For the compression behavior, the bilinear constitutive model was employed. The initial Young's modulus was assigned with the reduction factor (γ) until the compressive strain developed beyond $-\varepsilon_{ITZ}$ that refer to the crushing of ITZ under compression. Because the coarse aggregate comes into contact with mortar after crushing of ITZ, Young's modulus of ITZ is an average value of mortar and aggregate. For the shear behavior of ITZ, a similar constitutive model of shear spring for mortar was assigned. The internal friction was set to the same as mortar (37°), whereas the reduction factor (β) was introduced to other parameters for shear. Note that the reduction factors were obtained from the calibration process based on the existing experiment.

Because concrete must undergo the pre-drying and rewetting process along with the liquid water uptake, the hysteresis of stress-strain was carefully assigned for constitutive models of normal and shear springs to reproduce the volumetric change with respect to the moisture content in concrete. In addition, it should be noted that the spring parameters in the RBSM could not be directly adopted from the macroscopic properties of the material (Yamamoto et al., 2008). For the mesoscale RBSM, parameters used for mortar, aggregate, and ITZ must be calibrated from the macroscopic properties to appropriately assign parameters for springs in RBSM. The additional details of the constitutive models for mesoscale RBSM, their hysteresis, and calibration factors were comprehensively elucidated in the previous study (Sasano & Maruyama, 2021).

2.3 Mechanical property changes of concrete

The mechanical property change (MPC) of concrete with the moisture content has been reported by various studies and accentuated as the key factor for the deterioration of concrete due to the drying process. The experimental study on the microstructure of cement paste (Maruyama et al., 2019; Maruyama, Nishioka, et al., 2014; Maruyama, Sasano, et al., 2014) indicated that the dynamic change of pore structure regarding rearrangement of C-S-H structure during water movement is the key phenomena. Furthermore, the mesoscale numerical investigation (Sasano & Maruyama, 2021) clarified that an uneven deformation between cement paste and aggregate induces the microcrack, then alters the change in mechanical properties along with the microstructural change of cement paste. Therefore, the MPC of cement paste must be introduced to the constitutive model. In this study, the MPC of concrete was assigned based on the previous experiment (Maruyama, Sasano, et al., 2014) that used a similar composition of concrete. The alteration of compressive strength and Young's modulus of cement paste under several drying conditions were used as the residual ratio for the mechanical properties of the springs. The alteration of tensile strength, cohesion, and fracture energy was also considered by using the same residual ratio of compressive strength. The additional details of the input parameters for the MPC of mortar were described in the previous study (Sasano & Maruyama, 2021).

2.4 Time-dependent microcrack model

To consider the MPC of mortar in RBSM, the constitutive models were updated based on mechanical properties alternated along with the moisture content. However, updating of constitutive model insufficiently reproduces the impact of MPC and might cause an inappropriate stress-strain path. Thus, the time-dependent microcrack (TDM) model, which has been developed to consider the impact of MPC under the hardening and drying process (Maruyama et al., 2006; Sasano & Maruyama, 2021; Srimook et al., 2023), was employed to introduce the plastic deformation occurred throughout the history of the material. The concept of the TDM model is shifting the origin of the constitutive models after updating the mechanical properties due to the change in moisture content. The details of the TDM model were comprehensively elucidated in our previous studies.

2.5 Modeling of anomalous moisture transport in cracked concrete

In this study, anomalous moisture transport was introduced based on the concept of microstructure change and rapid absorption through cracks to quantitatively evaluate the liquid water uptake in cracked concrete. The details of the governing equations and numerical models for the aforementioned phenomena were elucidated in the following section.

(1) Moisture transport in TNM

In the TNM, the moisture transport in porous media like cement-based material was governed based on mass conservative law under the control volume, and the matrix form was derived by minimization of strain energy (Logan, 2007). Based on the TNM, the diffusion of moisture and evaporation at the concrete surface were reproduced by the governing and boundary equations as expressed in Eqs. (1) and (2).

$$\frac{1}{\omega}\frac{\partial R}{\partial t} = \frac{\partial}{\partial x}\left(D(R)\frac{\partial R}{\partial x}\right) + \dot{W} \tag{1}$$

$$\frac{\partial R}{\partial n} + \frac{\alpha_D D(R)}{d_{env}}(R - R_{env}) = 0 \tag{2}$$

Where R is the relative water content (-), x is the displacement along the axial direction of truss element (m), D(R) is the moisture transfer coefficient that depends on the relative water content in concrete (mm^2/s), and $\dot{W}$ is water consumption by hydration of cement (g/mm^3), which was neglected in this study. The moisture evaporation rate was determined based on the diffusion coefficient ($D(R)$) and virtual distance for water movement from the matrix to the environment (d_{env}). The virtual distance was used to represent the boundary condition of water transfer from the matrix to the environment (mm), which was determined by a previous study (Maruyama et al., 2011). α_D is fitted constant for the diffusion rate.

(2) Numerical implementation for mesoscale TNM

Fig. 2 shows the modeling of moisture transport for mesoscale TNM. The internal and boundary truss elements were assigned for mortar and coarse aggregate phases, which have different moisture transport properties. Because the ITZ phase was introduced to represent the weakness of concrete in the mechanical aspect, the influence of the ITZ phase, which is considered as the coarser pore structure compared to the mortar phase, should be considered for the diffusion process.

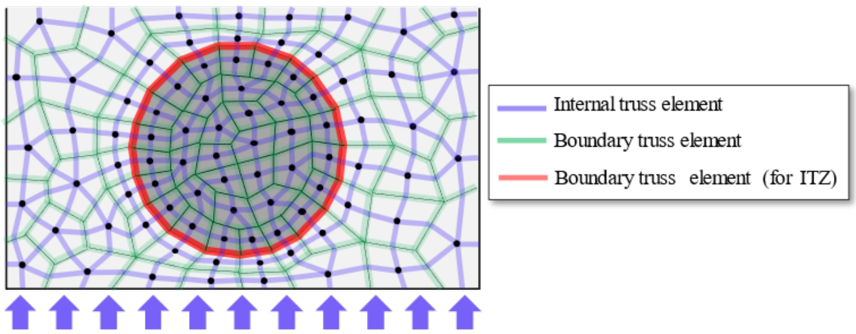

Fig. 2. Moisture transport for mesoscale truss-network model (TNM)

Owing to the coarser pore structure of ITZ, which might accelerate the moisture transport around aggregate, the boundary truss element at the interface between mortar and coarse aggregate was considered an ITZ zone. Before cracking, the area and volumetric of the boundary truss element for ITZ were assigned based on the ITZ's thickness (**Table** 2). After cracking, the moisture transport through cracks was assumed to be dominant, thus, the boundary truss element for ITZ considers the moisture transport through cracks as usual.

(3) Dynamic microstructural change model for anomalous moisture transport

To quantitatively evaluate the anomalous moisture transport, this study implemented the dynamic microstructural change model that introduces the anomalous behavior based on the microstructure data investigated by Nuclear Magnetic resonance (NMR) (Gajewicz et al., 2016; Janota et al., 2022; Kiran et al., 2020, 2021; McDonald et al., 2020). The NMR studies on liquid water uptake reported that the redistribution of absorbed water gradually occurred in the C-S-H structure, then induced the change in the pore system (Fig. 3(a)). Because the diffusivity of porous media depends on the pore size, the total diffusivity was also gradually altered along with the sorption and absorption process as shown in Fig. 3(b).

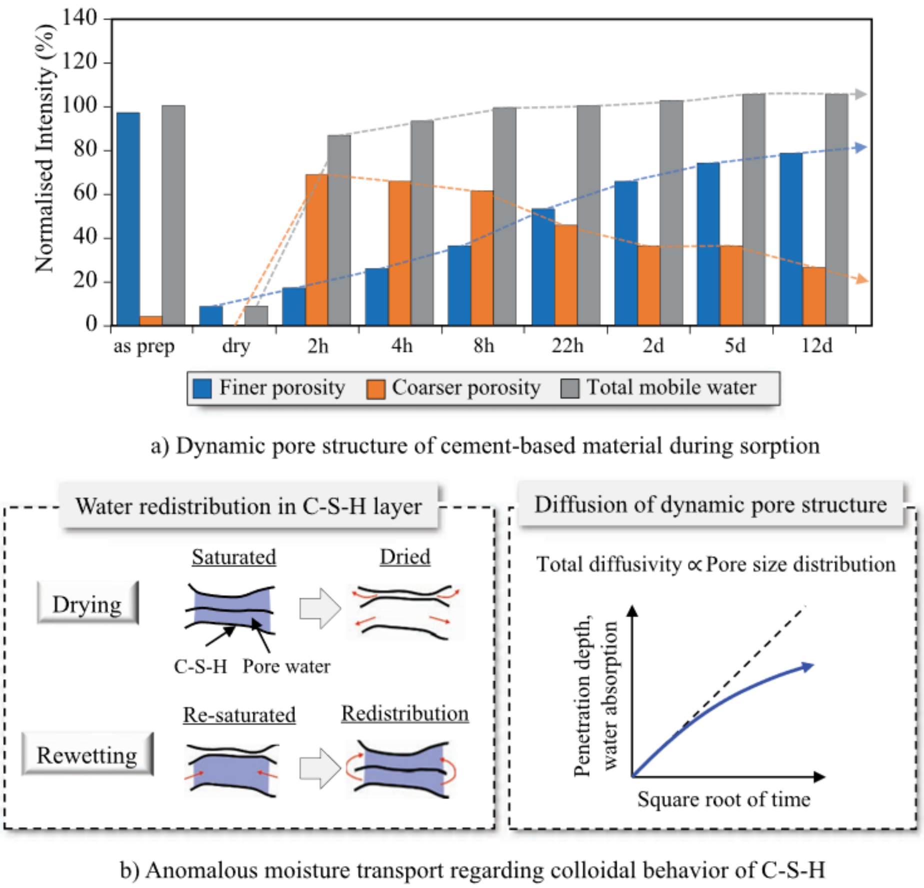

Fig. 3. Microstructural change of C-S-H structure and anomalous moisture transport in cement-based material (Gajewicz et al., 2016; Janota et al., 2022; Kiran et al., 2020; McDonald et al., 2020)

Fig. 4 shows the schematic diagram of the dynamic microstructural change model adopted for the mortar and ITZ phases. With the dynamic microstructural change model originated by (McDonald et al., 2020), the diffusion coefficient, which depends on dynamic microstructure (pore size distribution), saturation degree, and temperature, was determined as expressed by Eqs. (3)-(7). Owing to the rearrangement of the C-S-H layer with respect to the moisture content, the equilibrium pore size distribution at the given saturation degree was assigned based on NMR results (Table 2). Then, the dynamic microstructure (pore fraction) regarding the water redistribution in the C-S-H layer was reproduced based on the pore relaxation time constant, which was found to depend on composition, temperature, and pre-dried process, as expressed in Eqs. (3) and (4). Note that the dynamic microstructural change must rely on the criteria that the total pore fraction must be always equal to one (Eq. (5)). Regarding the effect of saturation degree, the saturation term of each pore was determined by assuming that water fills the smaller pores first and then fills the larger pores respectively. Finally, the total diffusion coefficient was determined as the summation of the diffusion coefficient of each pore fraction.

$$\frac{d\phi_i}{dt} = \frac{\phi_{i,n}^0 - \phi_{i,n-1}}{\tau_i} \quad ; \; i \in [il, gel, cap] \tag{3}$$

$$\phi_{i,n} = \phi_{i,n-1} + d\phi_i \quad ; \; i \in [il, gel, cap] \tag{4}$$

$$\phi_{il,n} + \phi_{gel,n} + \phi_{cap,n} = 1 \tag{5}$$

$$\begin{array}{l} \left.\begin{array}{r} s_{il} = S \\ s_{gel,cap} = 0 \end{array}\right\} \; S \le \phi_{il,n} \\ \left.\begin{array}{r} s_{il} = \phi_{il,n} \\ s_{gel} = S - \phi_{il,n} \\ s_{cap} = 0 \end{array}\right\} \; \phi_{il,n} \le S \le \phi_{il,n} + \phi_{gel,n} \\ \left.\begin{array}{r} s_{il,gel} = \phi_{(il,gel),n} \\ s_{cap} = S - \phi_{il,n} - \phi_{gel,n} \end{array}\right\} \; \phi_{il,n} + \phi_{gel,n} \le S \le \phi_{il,n} + \phi_{gel,n} + \phi_{cap,n} \end{array} \tag{6}$$

$$D(\phi, S) = \phi_{il,n} D_{il} \frac{e^{\frac{s_{il}}{\phi_{il,n}}}}{e} + \sum \phi_{i,n} D_i \frac{e^{\frac{s_i}{\phi_{i,n}}} - 1}{e - 1} \quad ; \; i \in [\, gel, cap] \tag{7}$$

where $d\phi_i/dt$ is an incremental pore fraction on each pore with an elapsed time, $\phi_{i,n}^0$, $\phi_{i,n-1}$, and $\phi_{i,n}$ are equilibrium pore fractions at a current step, relative pore fractions from the previous step, and relative pore fractions from the current step, respectively. τ_i is the pore relaxation time constant that was assumed to be equal for all types of pores, $D(\phi, S)$ is the total diffusion coefficient, D_{il} is the diffusion coefficient of each pore at full saturation state, S and S_i are the total and individual relative saturation degrees of each pore.

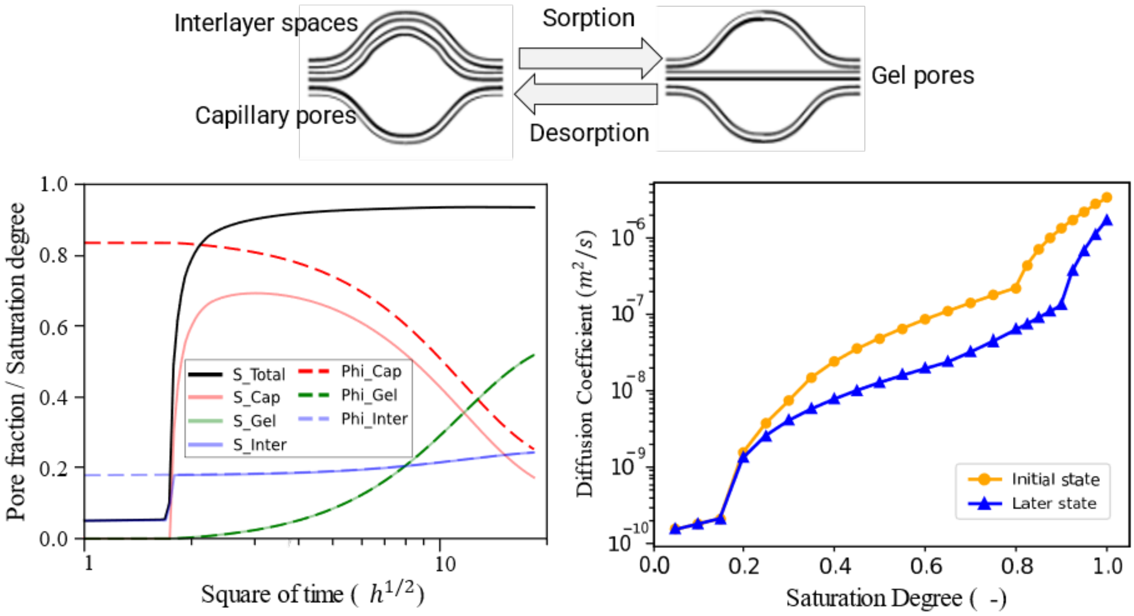

Fig. 4. Dynamic microstructural change model (Janota et al., 2022; McDonald et al., 2020)

(4) Volumetric change of concrete

The change in moisture content induces the volumetric change of concrete, which causes the MPC and microcracks due to an uneven deformation between mortar and coarse aggregate. In addition, our previous study (Srimook & Maruyama, 2023a) found that the concrete expansion during the rewetting process causes the closure of cracks. Therefore, the volumetric change of concrete must be appropriately introduced to clarify the alteration of structural performance and durability of concrete.

In this study, the volumetric change model of cement-based material was newly proposed. The volumetric change of the mortar phase was introduced based on the amount of gel and interlayer water related to the colloidal behavior of the C-S-H structure as shown in **Fig**. 5. Currently, there is no physical evidence to support this concept. However, the study based on the microstructure of cement paste observed a strong influence between microstructural change and shrinkage deformation (Maruyama et al., 2019; Maruyama, Nishioka, et al., 2014). The shrinkage mechanism should rely on the alteration of the pore system and disjoining (hydration) pressure according to the change in the C-S-H structure with moisture content. To accentuate the volumetric change of cement paste (especially expansion-induced closure of crack), the moisture transport and volumetric change of aggregates were neglected by assuming that aggregates have no pores.

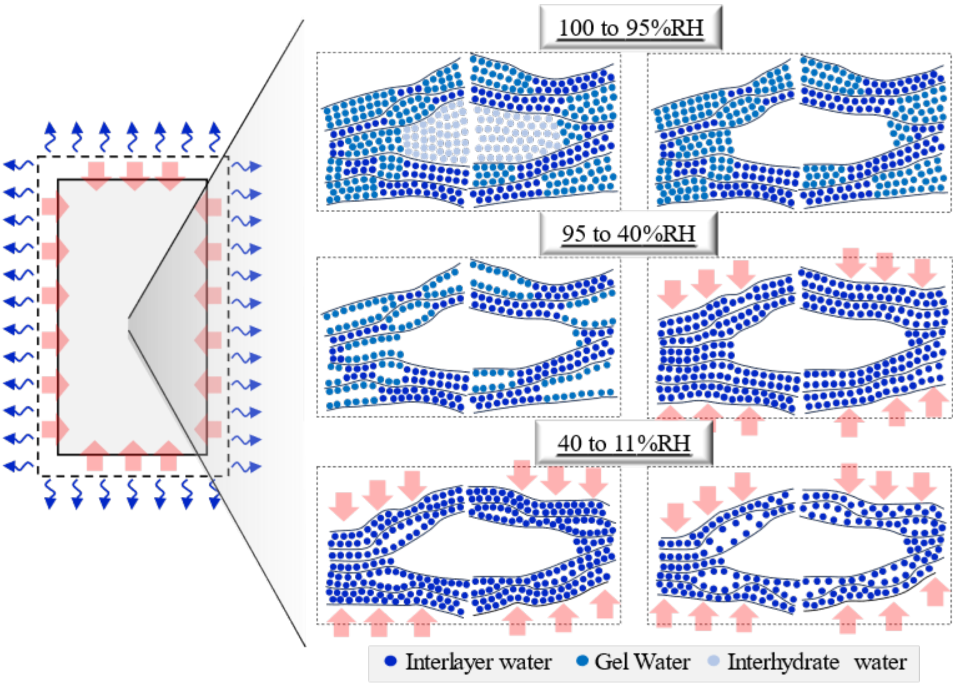

Fig. 5. Volumetric change model based on microstructural change of cement paste. Regarding the colloidal behavior of the C-S-H structure, the volume change of cement-based materials linearly alters with the water molecules surrounding the C-S-H structure (interlayer space and gel pores).

(5) Modeling of moisture transport through cracks in concrete

For concrete, microcracks according to an uneven deformation between cement paste and aggregate have been reported as the accelerator of moisture transport in concrete. Owing to the influence of cracking on moisture transport, various numerical models were proposed to reproduce the rapid absorption based on diffusion processes like cubic law. Nevertheless, the experimental study based on neutron imaging (P. Zhang et al., 2010) reported that the rapid absorption through cracks occurs within a few minutes followed by the water redistribution from the crack into a concrete matrix. Therefore, the cubic law solely could not reproduce the complex behavior mentioned above.

In this study, the rapid absorption through cracks and water redistribution were explicitly modeled the rapid absorption based on the numerical approach proposed by (Singla et al., 2022). The rapid absorption through cracks, which interconnect from the water source, was modeled based on the Lucas-Washburn equation (Eq. (8) represents the capillary absorption between parallel crack walls under the balancing of driving capillary force, retarding viscosity, gravity, and initial force (Hamraoui & Nylander, 2002).

$$\left(\frac{2\beta_m}{r}+\frac{y}{\frac{r\beta_w}{2}+\frac{r^2}{8\mu}}\right)\dot{y}=p_{c0}(1-\beta_s)-\rho g y sinc(\varphi) \qquad (8)$$

where β_m is the correction factor for dynamic contact angle, r is the radius of the capillary, y is the capillary rise, β_w is the correction factor for the wall slip, μ is the dynamic viscosity, β_s is the correction factor for the stick-slip behavior, ρ the density of the liquid (water), φ is the inclination angle of the capillary, g is the acceleration due to gravity, p_{c0} is the capillary pressure determined as $2\gamma\cos(\alpha_0)/r$, γ is the surface tension, and α_0 is the liquid-solid contact angle.

By using the Crank-Nicolson procedure, the Lucas-Washburn equation was discretized in time and the modified Lucas-Washburn equation, which was derived by (Gardner et al., 2012), is expressed in Eqs. (9)-(14).

$$z_{n+1} = z_n + \frac{\Delta t}{2}(\dot{z}_n + \dot{z}_{n+1}) \tag{9}$$

$$\frac{2}{\Delta t} z_{n+1}^2 + \left(\frac{2}{\Delta t}k_1 k_2 - \frac{2}{\Delta t}z_n - \frac{k_2 k_3 - k_2 k_4 z_n}{k_1 k_2 + z_n} + k_2 k_4\right) z_{n+1} - \left(\frac{2}{\Delta t}k_1 k_2 z_n + \frac{k_1(k_2 k_3 - k_2 k_4 z_n)}{k_1 k_2 + z_n} + k_2 k_3\right) = 0 \tag{10}$$

$$k_1 = \frac{2\beta_m}{2} \tag{11}$$

$$k_2 = \frac{r\beta_w}{2} + \frac{r^2}{8\mu} \tag{12}$$

$$k_3 = p_{c0}(1 - \beta_s) \tag{13}$$

$$k_4 = \rho g \sin(\phi) \tag{14}$$

where z_n and z_{n+1} is the capillary rise height in the current and next step (mm), Δt is the elapsed time (s), k_1, k_2, k_3, and k_4 are the term of capillary absorption that was simplified for the derivative of the equations.

To introduce the rapid absorption through cracks in the TNM, the modified Lucas-Washburn equation was introduced for boundary truss elements on cracking paths interconnected from water sources. The capillary rise height was determined based on the crack aperture under a very small incremental time. Once the capillary height in cracks was computed and found that capillary height develops beyond the location of truss nodes on the crack surface, the boundary condition of truss nodes was changed to absorbed surface in order to introduce the water redistribution from saturated cracks to unsaturated cement paste matrix. The schematic diagram for the calculation of the capillary rise height and changing the boundary condition are described in **Fig.** 6.

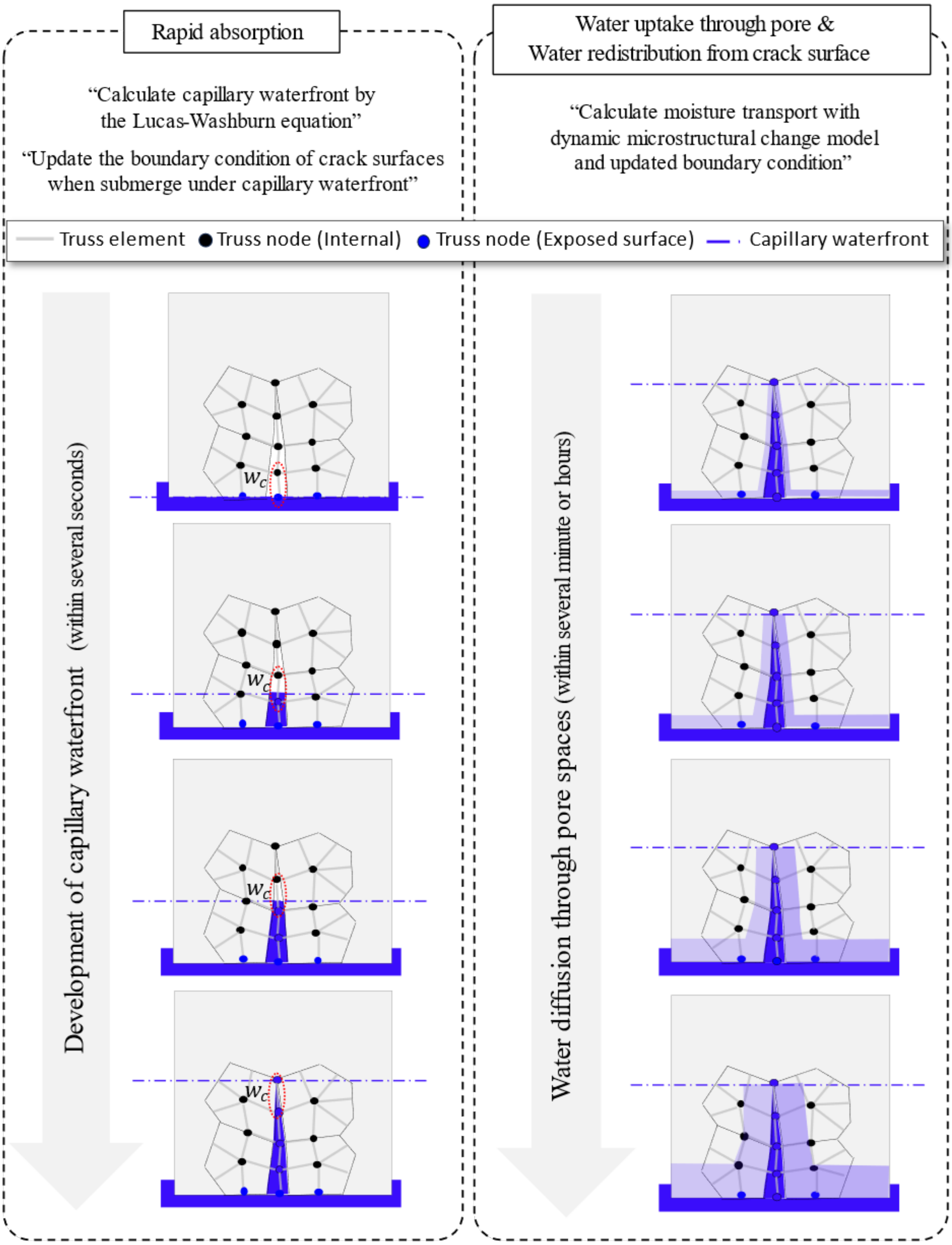

Fig. 6. Schematic diagram of calculation of capillary rise height for rapid absorption process and changing the boundary condition for water redistribution process

For cracks that do not connect from the absorbed surface or are located beyond capillary rise height, moisture transport through cracks was modeled by the cubic law, which was validated by previous studies (Singla et al., 2022; L. Wang et al., 2016; Witherspoon et al., 1980). The diffusion coefficient of the boundary truss element was determined by a crack aperture as shown in Eq. (15).

$$D_w^{cr}(S) = \frac{\xi p_r w^2}{12\mu} \cdot \frac{(1-m)}{m} \sqrt{S}\, [1-(1-S^{1/m})^m]^2\, S^{-1/m-1} [S^{-1/m}-1]^{-m} \tag{15}$$

where w is the equivalent crack width, ξ is the tortuosity factor, pr is the reference pressure (experimentally determined as 18.6237 N/mm2), m is the van Genuchten parameter (0.4396) and μ the viscosity of water.

2.6 Numerical flow for anomalous liquid water uptake in cracked concrete

To reproduce the anomalous liquid water uptake in cracked concrete and mechanical responses, the numerical flow was proposed as shown in **Fig.** 7.

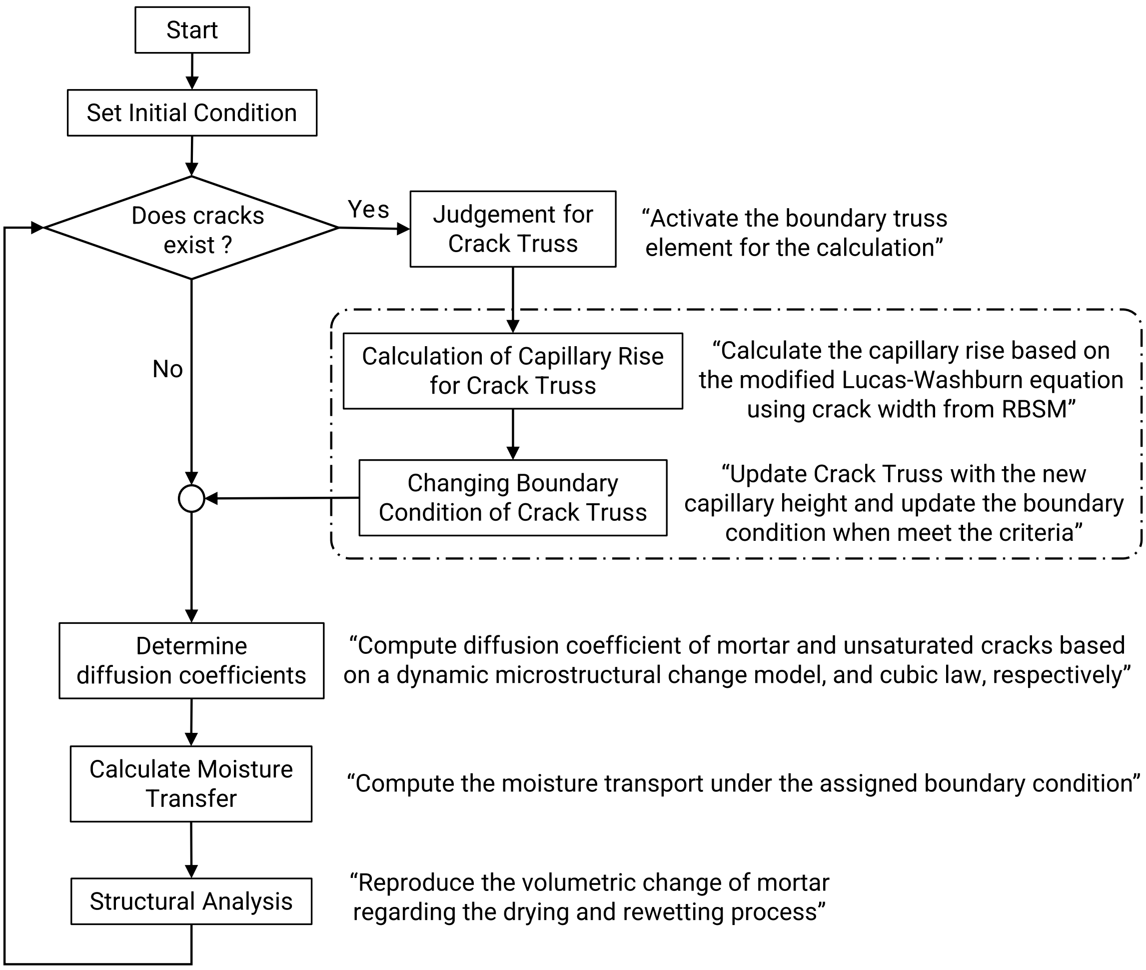

Fig. 7. Numerical flow for anomalous moisture transport and mechanical responses

In each step, the calculation starts with the identification of the crack truss (active boundary truss element on the crack surface). Afterward, the calculation of capillary absorption was performed for the crack truss, which contains the capillary front. The capillary height was determined and stored for each crack truss. Once the capillary height surpasses the top node of the crack truss, the top node will be considered as the absorbed surface. In addition, the capillary height was updated to the adjacent crack truss to consider the connectivity as described in the previous section. Noted that the changing of the boundary surface required a small incremental time (0.05 – 0.1 second) to gradually change the crack surface from the bottom part toward the tip of the cracks as shown in **Fig.** 6. Therefore, the incremental time for the diffusion process (generally, 60 seconds) was discretized to the small incremental time. With the small time incremental, the calculation of capillary rise was performed step based on the crack truss containing the front of capillary water. In order to ensure the equilibrium of the rapid absorption process, the iterative calculation loop was proposed for the boundary changing and transferring the calculated capillary height to the adjacent crack truss. The iterative continues until reaches the equilibrium state (no more updates for all crack trusses).

After determining the capillary rise height and the absorbed surface on the crack wall, moisture transport in cracked concrete was conducted with TNM. The diffusion coefficient of the mortar phase was computed based on the dynamic microstructural change model. In addition, the diffusion coefficient of unsaturated cracks was computed based on cubic law.

For the structural analysis, the moisture distribution obtained from TNM was used to determine the volumetric change of cement paste. The change in moisture content from the truss node at the boundary surface and shrinkage coefficient was used to introduce the initial strain of springs. Then, the internal stress and strain were determined based on the Newton-Raphson procedure. Since the drying process of the concrete sample is free of restraint conditions, the solution was considered to converge when the summation of internal stress is close to zero.

3. Numerical study on anomalous liquid water uptake in cracked concrete

The mesoscale numerical study on liquid water uptake in cracked concrete was conducted based on the reference experiment by our research group. The numerical implementation and material parameters used for mesoscale RBSM and TNM were assigned to represent the realistic condition. The validity of the proposed modeling approach was clarified based on a comparison between experimental and numerical results.

3.1 Introduction of reference experiment

The numerical study was conducted based on the experimental investigation of the liquid water uptake process in cracked concrete using the digital image correlation (DIC) method (Ogawa et al., 2023). Owing to the deformation of concrete during the rewetting process, the liquid water uptake process was investigated based on the 2D-strain distribution analyzed by the digital images recorded during the water uptake test.

In the reference experiment, the 100 × 100 mm concrete sample was cast with OPC and a water-to-cement ratio of 0.55. After the curing process, the well-hydrated OPC concrete was cut into 10 mm-thickness concrete slabs. The surface of the specimens was polished for both sides and then coated with the epoxy resin primer to provide the random pattern for the DIC method. The specimens were dried at 105 ˚C for 96 hours before conducting the liquid water uptake test for 168 hours. Throughout the pre-drying and water uptake experiment, digital images of the ransom pattern were recorded on the specimen surface, which is perpendicular to the immerse surface. Digital images were used to analyze the 2D-principal strain distribution by using the Vic-2D, which interpolates the intensity value distribution of the random pattern and determines the direction of deformation.

Based on the aforementioned approach, the 2D distribution of maximum and minimum principal strain was determined and used to visualize the expansion and shrinkage deformation, respectively. Because maximum principal strain indicates not only the mortar expansion but also the existence of cracks (Maruyama & Sasano, 2014), the penetration depth was determined based on the minimum principal strain, which reflects the strain of the material, especially when no interaction occurs. The minimum principal strain distribution after drying was averaged at each depth, and then the normalized curve was determined based on the strain distribution at the top of the specimen where water did not reach through the water uptake test. The penetration depth, which refers to the location of the capillary waterfront, was identified as the end of the steepest slope. The schematic diagram of the reference experiment is shown in **Fig.** 8. **Fig**. 9(a) shows the distribution of the post-dried maximum principal strain analyzed based on the DIC method. **Fig**. 9(b) shows the penetration depth development analyzed from the minimum principal strain throughout the water uptake test.

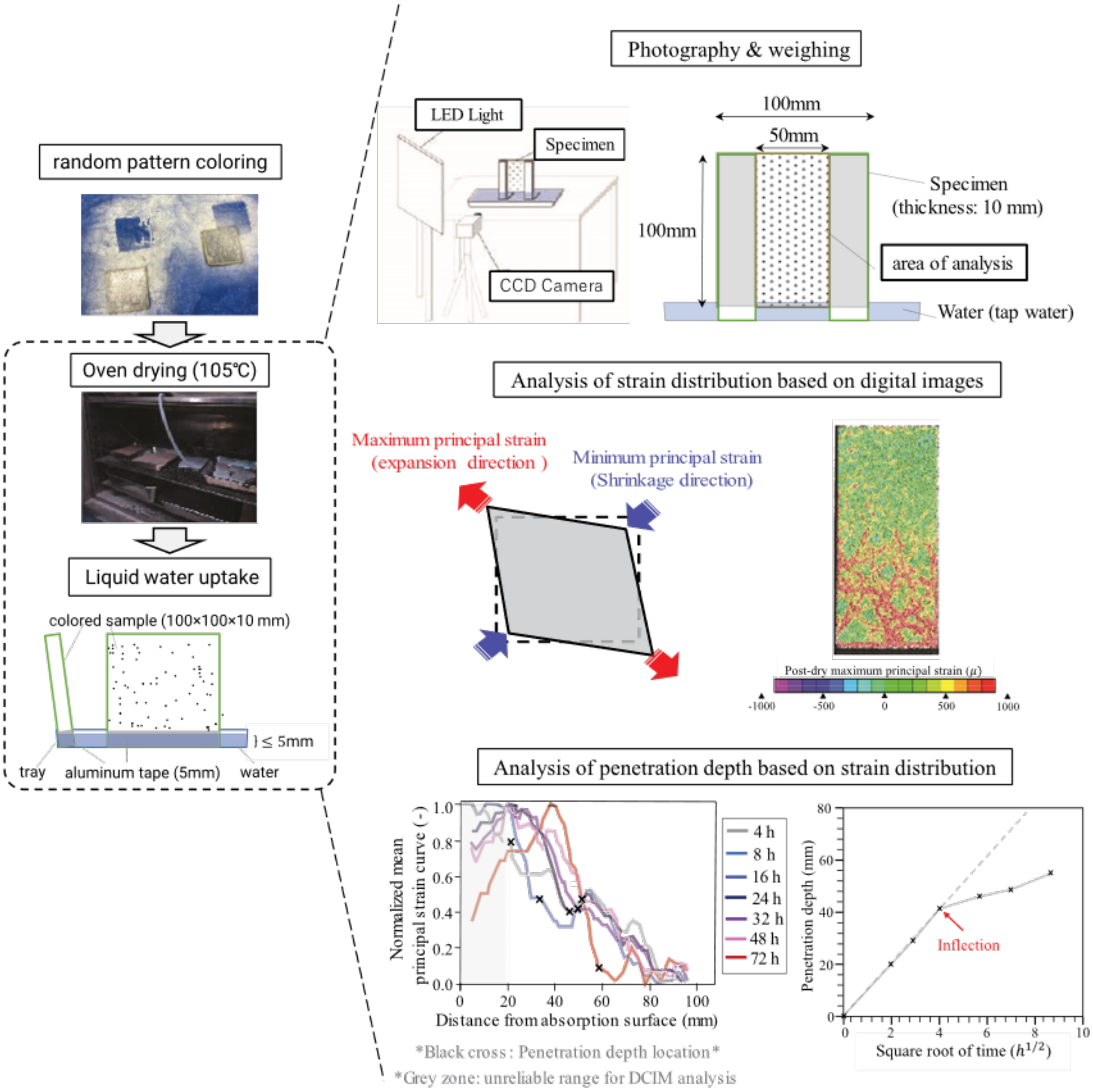

Fig. 8. Experimental investigation on liquid water uptake in concrete using digital image correlation (DIC) method (Ogawa et al., 2023)

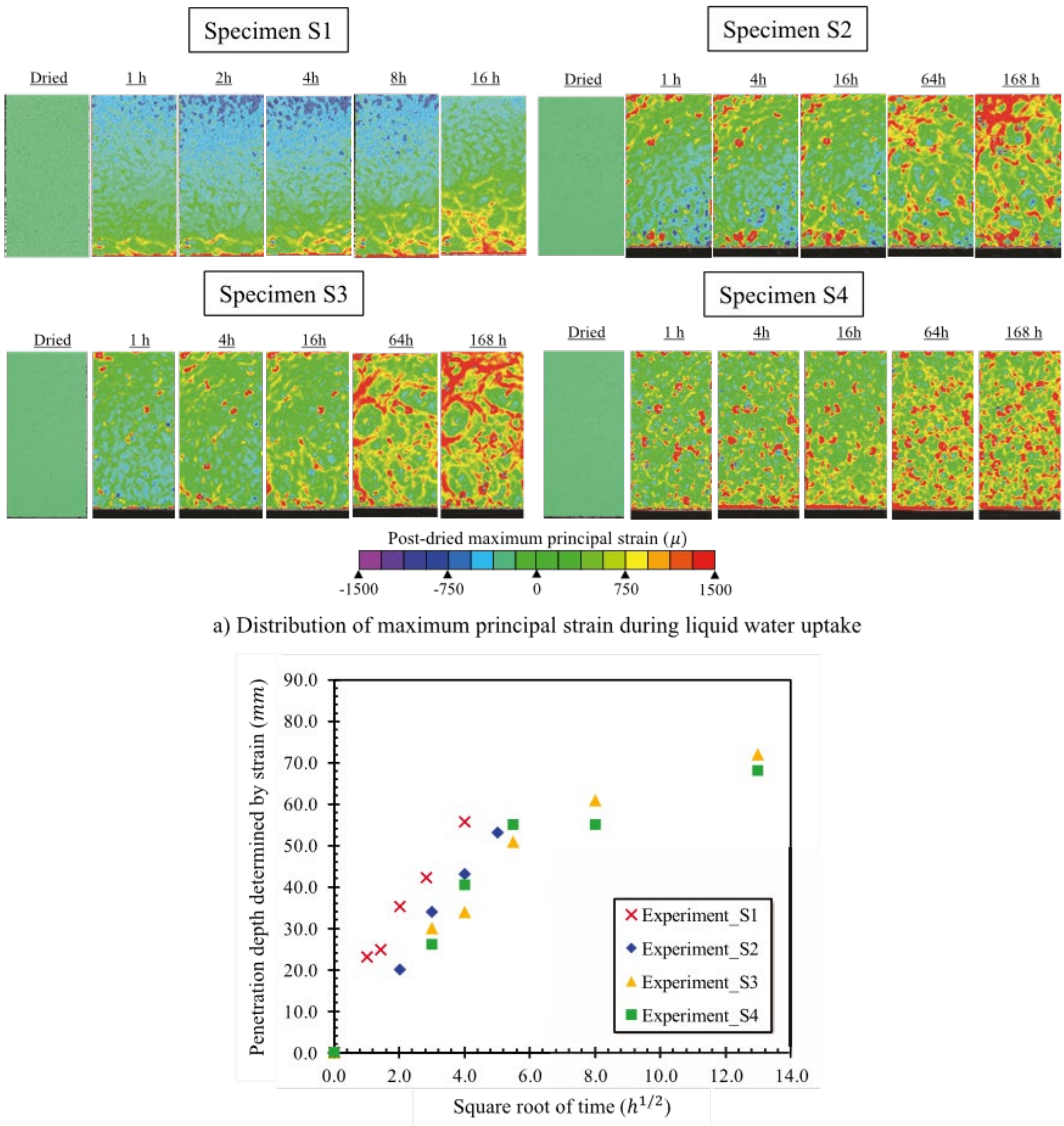

a) Distribution of maximum principal strain during liquid water uptake

b) Penetration depth development during liquid water uptake

Fig. 9. Liquid water uptake in concrete investigated by digital image correlation (DIC) method: (a) Maximum principal strain distribution and (b) penetration depth development along with liquid water uptake (Ogawa et al., 2023).

3.2 Additional details on the numerical implementation and materials parameters

(1) Mesh of reference specimen

The 100×100×10 mm concrete slab, which is a composite material of mortar, aggregate, and ITZ was meshed as shown in Fig. 1. The Voronoi mesh is composed of 17,956 elements, and the average element size is 2 mm. Note that coarse aggregates were meshed based on the spherical shape due to difficulties found in the meshing process. Although coarse aggregates used in this study are not in an irregular shape as that of the reference experiment, the maximum aggregate size and aggregate ratio were assigned based on the concrete mixture used in the reference experiment. The cumulative passing of aggregate size was assigned within the limited range following the Japanese Industrial Standard (JIS) as shown in **Fig.** 10.

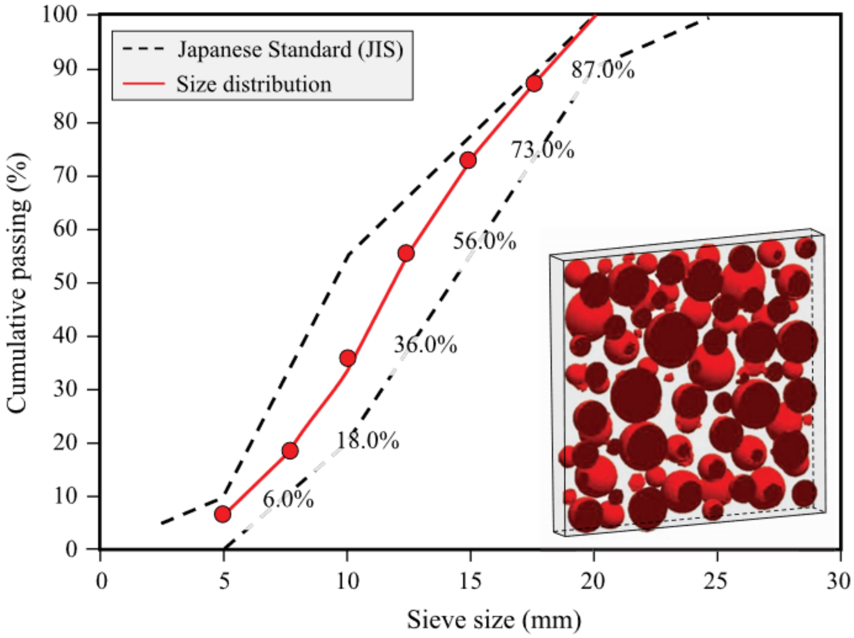

Fig. 10. Mesh of reference specimen and aggregate size distribution

(2) Material properties for mesoscale RBSM and TNM

Table 1 lists the 28-day mechanical properties used for the structural analysis. The mechanical property change of mortar was determined based on the 28-day mechanical properties, the residual ratio of Young's Modulus, and strength as described in section 2.3.

Table 1. Input mechanical properties for mortar and aggregate. The asterisk (*) refers to parameters given by empirical equations from previous experimental data. f_t, f_c, and $G_{ft}$of aggregate were referred from the previous study (Sasano & Maruyama, 2021).

	E_c (N/mm^2)	f_t (N/mm^2)	f_c (N/mm^2)	G_{ft} (N/mm)
Mortar	16,900	3.79*	46.6	0.0615*
Aggregate	70,000	10.0	150.0	0.0200

Table 2 lists the moisture transport properties used for the dynamic microstructural model. For the mortar phase, although there is no NMR data representing the microstructure for the reference specimen, the pore fraction used in this study was adopted from the previous NMR studies (Janota et al., 2022), which studied moisture transport in OPC. Note that the microstructural data could not be directly applied to the reference experiment regarding the differences in the w/c ratio, curing, and pre-condition process. However, from the calibration process, two fitted parameters were determined by the calibration process. From the calibration process, the fitted parameter of the total diffusion is equal to 0.1 and the pore relaxation time is 30 hours which is comparable to the NMR data and reference experiment.

In the reference experiment, concrete was cast by mixed crushed stone, and strain distribution analyzed by DIC indicated that the closure of cracks is caused by mortar expansion during the rewetting process. Therefore, this study assumed that aggregates are non-absorbed materials (no diffusion and volumetric change) in order to simplify the variation in moisture transport properties in the aggregate phase and accentuate the impact of the volumetric change on the crack closure process. Because ITZ was introduced as the coarser pore structure compared to the mortar phase, the diffusion coefficient of the ITZ phase was assumed to be 10 times greater than the mortar.

Table 2. Input moisture transfer properties for mortar phase.

Diffusion Coefficient of Mortar based on Dynamic Microstructural Change Mode

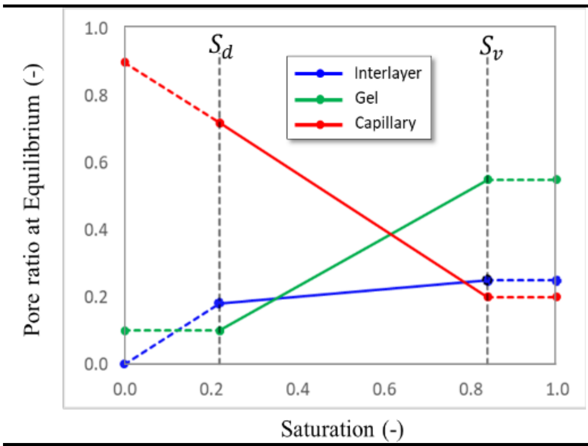

	S_d	S_v	τ (hr)
	0.220	0.840	30
	Interlayer	Gel	Capillary
$\phi_{Eq,d,i}$	0.180	0.100	0.720
$\phi_{Eq,v,i}$	0.250	0.550	0.200
n_i	1.0	1.0	1.0
D_i (m^2/s)	D_{Cap}/500	D_{Cap}/100	2.85E-7

The volume change ratio of mortar was assigned based empirical equation (Eq. (16)) obtained from the previous experiment (Maruyama, Sasano, et al., 2014) in order to reproduce the drying shrinkage and expansion strain along with the moisture transport in concrete.

$$\varepsilon_{sh,mor} = 5162 \cdot \Delta R^4 - 8726 \cdot \Delta R^3 + 4527 \cdot \Delta R^2 - 2733 \cdot \Delta R \qquad (16)$$

where $\varepsilon_{sh,mor}$ is the input mortar shrinkage for the concrete analysis (με), and ΔR is moisture loss from the saturation state (-). Regarding the volumetric change model based on the MCCP, the moisture loss was computed by the amount of water molecules surrounding the C-S-H structure (interlayer and gel water).

3.3 Numerical results

(1) Anomalous liquid water uptake in cracked concrete

The liquid water uptake in dried concrete, which contains microcracks perpendicular to the aggregate surface, was investigated based on the development of penetration depth with the square root of time. **Fig**. 11 shows the moisture distribution and penetration depth development obtained from the numerical study. From the moisture distribution (**Fig.** 11(a)), the liquid water uptake through cracked concrete according to capillary absorption was appropriately reproduced. Regarding the moisture distribution, the penetration depth, which refers to the top of the capillary front observed throughout the specimen, was determined and compared with the experimental results as shown in **Fig.** 11(b). The linear relationship between the penetration depth and square root of time could be reproduced at the initial stage. The deviation of the penetration depth from the linear relationship with the square root of time was reproduced around 16 to 30 hours.

Compared with experimental results, good agreements could be observed, except for specimen S1 which shows more rapid water absorption. Based on the principal strain data, the difference in S1 possibly comes from the rapid absorption through fine cracks, which seem to be more distributed and interconnect with each other. Nevertheless, the consistency of the numerical study with specimens S2, S3, and S4 adequately indicated the validity of the proposed modeling approach to reproduce the anomalous behavior.

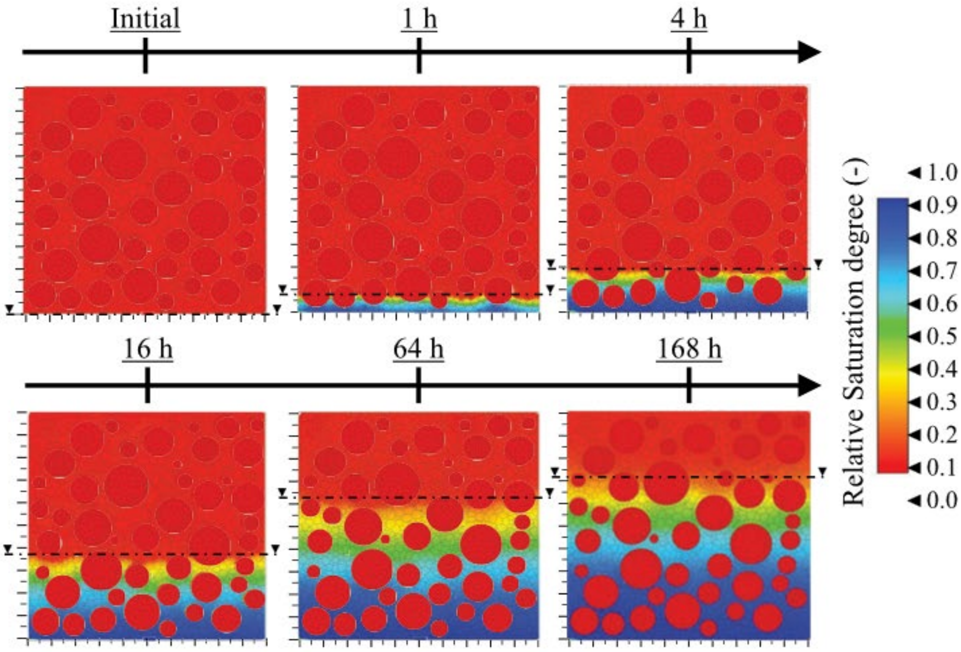

a) Moisture distribution during water uptake

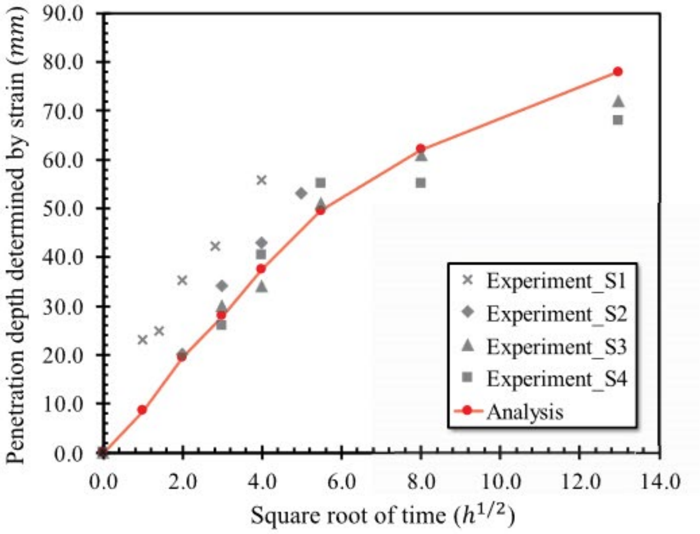

b) Penetration depth development determined by principal strain

Fig. 11. Anomalous liquid water uptake in cracked concrete

(2) Mechanical response according to liquid water uptake

The mechanical response along with the liquid water uptake was also investigated based on the development of concrete expansion. **Fig**. 12 shows the post-dried mechanical responses along with the liquid water uptake, which indicates the liquid water uptake progress regarding macroscopic deformation, and principal strain development in the mortar phase.

Note that the principal strain distribution in RBSM was not calculated directly from elemental strain because the element was considered as rigid particles. It was converted from the principal stress determined based on the spring stress. Because several cracks occurred in the mortar, the principal strain determined by the aforementioned procedure might be underestimated. However, from the crack distribution in Fig. 12, the crack width regarding the pre-drying process is quite small (1 to 9 microns), thus, the small discrepancy will not significantly affect the calculation results.

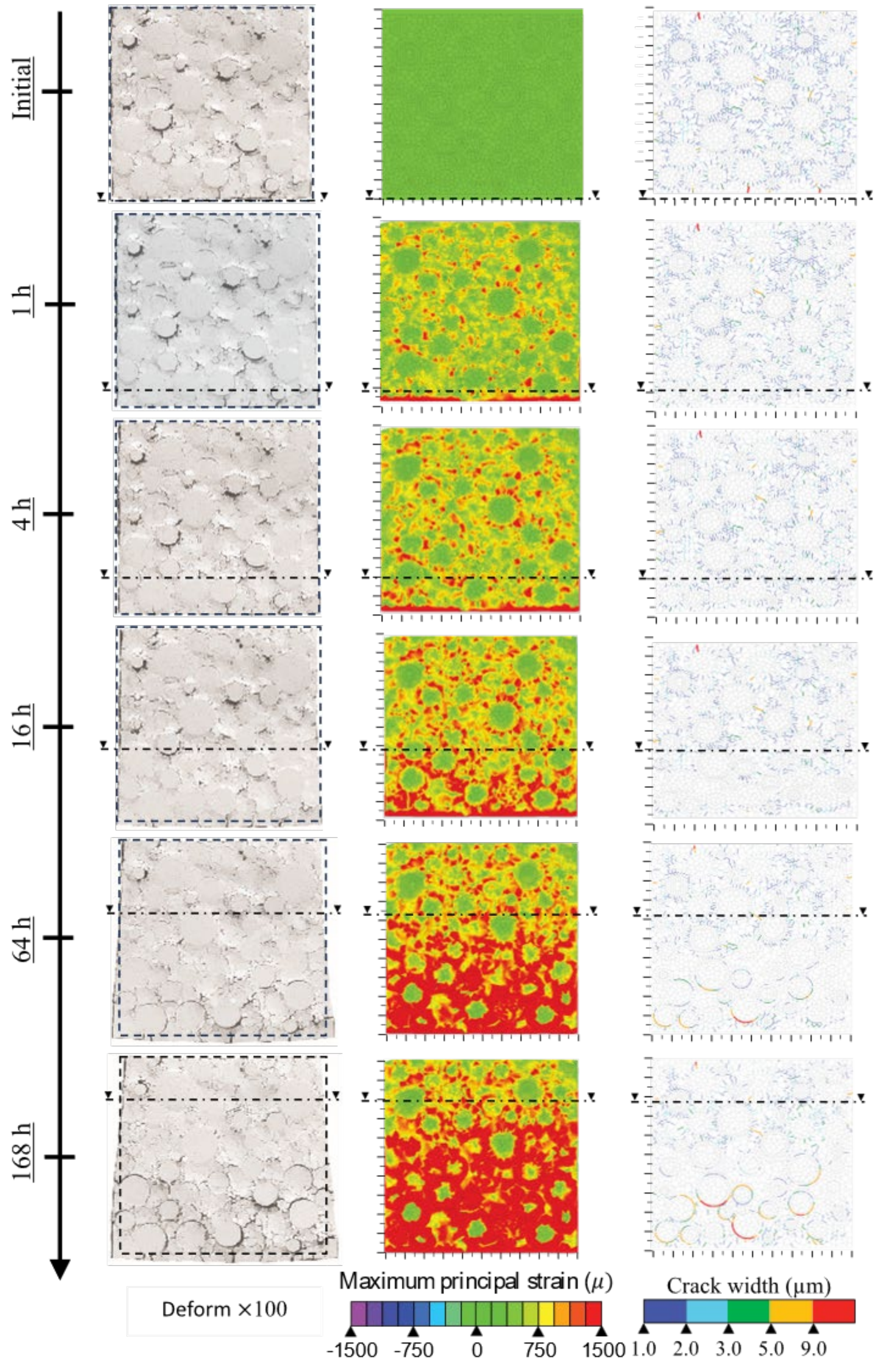

Fig. 12. Mechanical responses according to liquid water uptake

Compared to the reference experiment (Fig. 9), the development of the principal strain analyzed by the numerical study seems to be consistent with experimental results. Even though the expansion of mortar was observed above the saturated area at the bottom part, the principal strain developed in accordance with the moisture distribution during liquid water uptake. A similar distribution of principal strain development was observed for several specimens (S2, S3, and S4). In addition, at the early period, the principal strain distribution in the reference experiment indicated that the expansion occurred throughout the specimen similar to that of numerical results. Only specimen S1 shows the different distribution of the principal strain, which clearly shows the progress of liquid water uptake progress. However, the water uptake rapidly occurred compared to other specimens.

Owing to the capability of RBSM, the crack distribution was visualized during the liquid water uptake as shown in Fig. 12. The alteration of cracks, which occur in accordance with mortar expansion during the rewetting process, was observed. The drying shrinkage cracks, which are perpendicular to the aggregate surface, gradually disappeared along with the mortar expansion. Nevertheless, some cracks remain near the surface area and the expansive cracks, which are parallel to the aggregate, occurred near the saturation state. The alteration of cracks in the saturated area was not reported in the reference experiment because it is quite difficult to distinguish between crack closure and mortar expansion from the principal strain for both the DIC method and RBSM.

In the reference experiment, the red pattern above saturated was pointed out as the existence of entrapped air that was exposed to the specimen surface. Nevertheless, a similar pattern was observed even if the influence of entrapped air was not accentuated in this study. From the crack distribution analyzed by the numerical study, it seems that the development of principal strain above the saturated area corresponds with the alteration of microcracks, which are perpendicular to the aggregate surface. Since specimens encountered the severe drying process, liquid water uptake in dried concrete induces the alteration of cracks regarding the instability under the free expansion. A similar observation was also observed in macroscopic deformation (Fig. 15) and stress distribution (Fig. 16) showing the sudden expansion for the entire specimen and stress relief at the initial stage of the water uptake. The details of macroscopic deformation and stress distribution during the water uptake will be elucidated in the latter sections.

Note that there are differences between the numerical study and reference experiment, which were assumed based on previous studies, such as microstructural data, aggregate shape, and distribution. These differences might affect the liquid water uptake, especially the liquid water uptake through cracks that depend on the connectivity of the drying shrinkage crack. The numerical study based on the realistic aggregate shape and distribution must be further investigated. Nevertheless, it is worth mentioning that the modeling approach adequately reproduces the rapid absorption through surface cracks as well as the closure of cracks regarding the expansion of mortar (cement paste) during the rewetting process.

4. Discussion

The anomalous moisture transport and mechanical responses in concrete are complex behaviors because several phenomena are involved. Therefore, it is quite difficult to clarify the mechanism by an experiment. Owing to the validity of the proposed modeling approach, further numerical investigation was performed to clarify the mechanism of anomalous behavior, the effect of microstructural change on volume change of cement pates, and mortar expansion-induced closure of cracks in the following section.

4.1 Anomalous behavior of moisture transport in cracked concrete

The anomalous behavior of moisture transport in concrete was reported as the consequence of various phenomena. The NMR study on the microstructure of cement paste clarified that the anomalous behavior is caused by the colloidal behavior of C-S-H (Janota et al., 2022;

McDonald et al., 2020). Whereas the study based on fluorescence imaging reported that the rapid absorption through cracks influences anomalous behavior (Wu et al., 2019). To clarify the mechanism, further numerical investigation was performed as listed in **Table** 3**,** and compared between each case to clarify the contribution of each phenomenon as shown in **Fig.** 13.

Table 3. List of calculations for clarifying anomalous moisture transport in cracked concrete.

	Numerical cases			
	A: Standard	B: without MCCP	C: without cracks	D: Traditional
MCCP	✓		✓	
Microcracks	✓	✓		

Regarding the comparison of penetration depth development, the differences observed from cases A and B clarified the influence of MCCP. The deviation from the linear relationship at the later stage is mainly caused by the alteration of total diffusivity in the dynamic pore structure of cement paste. This is because the large number of coarse pores, which was induced from the collapse of the C-S-H during the pre-drying process, gradually transforms into fine pores with the pore relaxation rate as evidenced by NMR data (Janota et al., 2022; McDonald et al., 2020). Regarding the aforementioned process, the penetration depth gradually deviates from the linear relationship as shown in **Fig.** 13 (solid red and dashed blue lines).

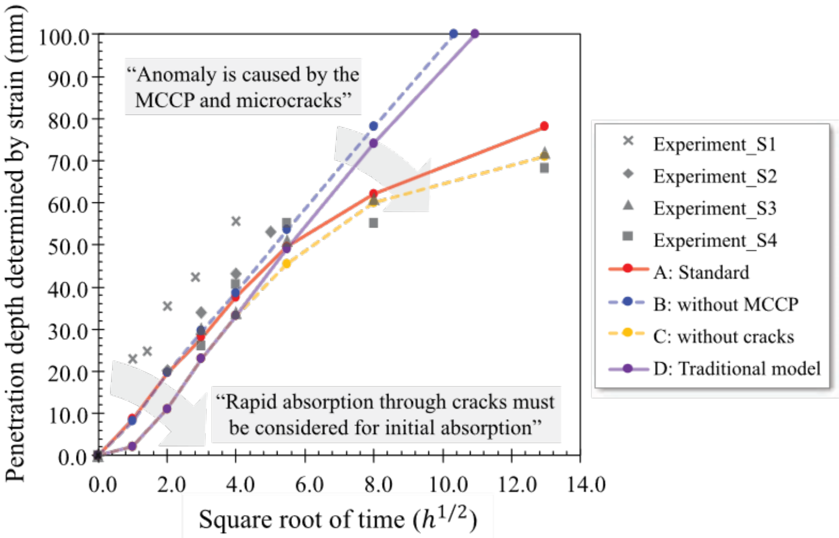

Fig. 13. Mechanism of anomalous liquid water uptake in cracked concrete

The influence of cracks was investigated based on the comparison between cases A and C. The different development of penetration depth (red solid and dashed yellow line) indicated that drying shrinkage cracks significantly influence the water absorption at the initial stage, whereas a little influence was observed at the later stage according to a similar development curve. Without cracks, the anomalous behavior of moisture transport was observed regarding the slower absorption process at the initial stage. The inflection point was observed at 1 hour, and afterward, the penetration depth developed at the same rate as the standard case. Thus, it is worth mentioning that drying shrinkage cracks significantly affect the initial absorption process. This phenomenon is consistent with the previous experiment, which studied the anomalous water absorption in cement-based materials under various pre-conditioning regimes (Wu et al., 2019). By using the fluorescence imaging technique, the rapid absorption through surface cracks was evidenced which was also observed by our numerical study (**Fig.** 14). The anomalous behavior was reported based on the change in slope of cumulative water absorption, which was found to be correlated with the drying damage identified by the quantity of microcracks (e.g., average crack width, total crack length, and crack density).

The contribution of both phenomena was investigated based on the comparison between cases A and D which was calculated based on the proposed and traditional modeling approaches. From the comparison between numerical cases A and D, the large difference in penetration depth development indicated the importance of MCCP and microcracks. From the comparison with the experiment, the penetration depth was underestimated at the initial absorption and overestimated at the later absorption. In other words, it is worth mentioning that both MCCP and rapid absorption through cracks must be considered to represent the realistic moisture transport in dried concrete.

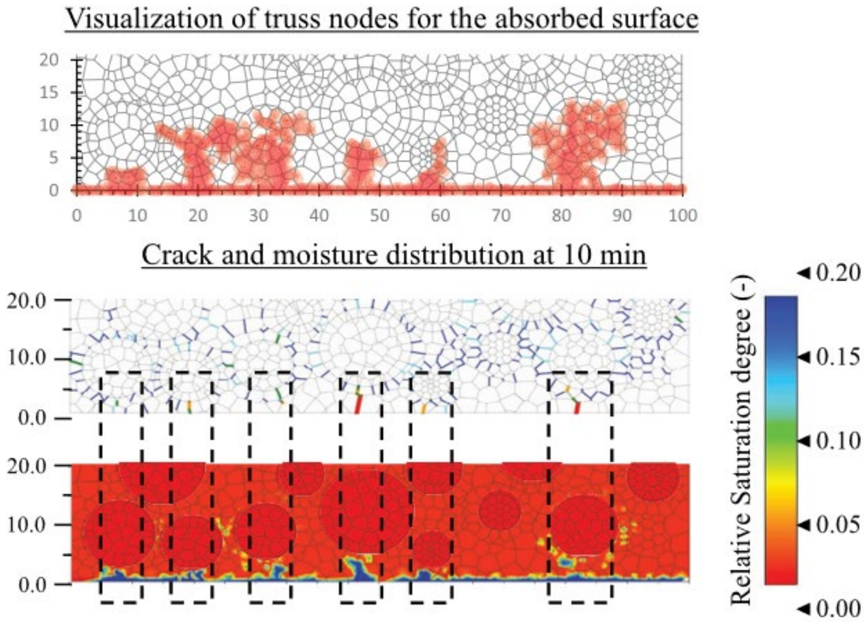

Fig. 14. Rapid absorption through surface cracks

4.2 Volumetric change of cement pastes regarding microstructural change

The MCCP is a key phenomenon that induces not only the anomalous behavior in moisture transport but also the mechanical response of concrete. Because the mortar expansion induced the closure of cracks as observed in the previous studies (Srimook & Maruyama, 2023a) and reference experiment (Ogawa et al., 2023), the volumetric change of mortar must be appropriately reproduced. Thus, in this study, the volumetric change model based on MCCP was newly proposed and introduced for the mortar phase.

To clarify the influence of microstructural change on volumetric change, the concrete expansion (lateral and vertical deformation) was investigated by comparing the numerical results from traditional and microstructural change models as shown in **Fig.** 15. The significant difference in the concrete expansion implied the influence of MCCP. Owing to MCCP that gradually occurs based on the pore relaxation process, gradual expansion was observed for the proposed model instead of sudden expansion by the traditional model. The aforementioned characteristic is consistent with the previous experiment (Alderete et al., 2019), which studied the influence of concrete swelling on anomalous capillary water uptake. The horizontal and vertical strain measured by the strain gauge clarified that the concrete gradually swells from the surface contact with water until reaching the equilibrium. The consistency of the gradual deformation implied that the volumetric change of cement-based material depends on the

MCCP. The rate of volumetric change also relies on the water redistribution in the C-S-H structure. Nevertheless, there are differences in the deformation compared to numerical results.

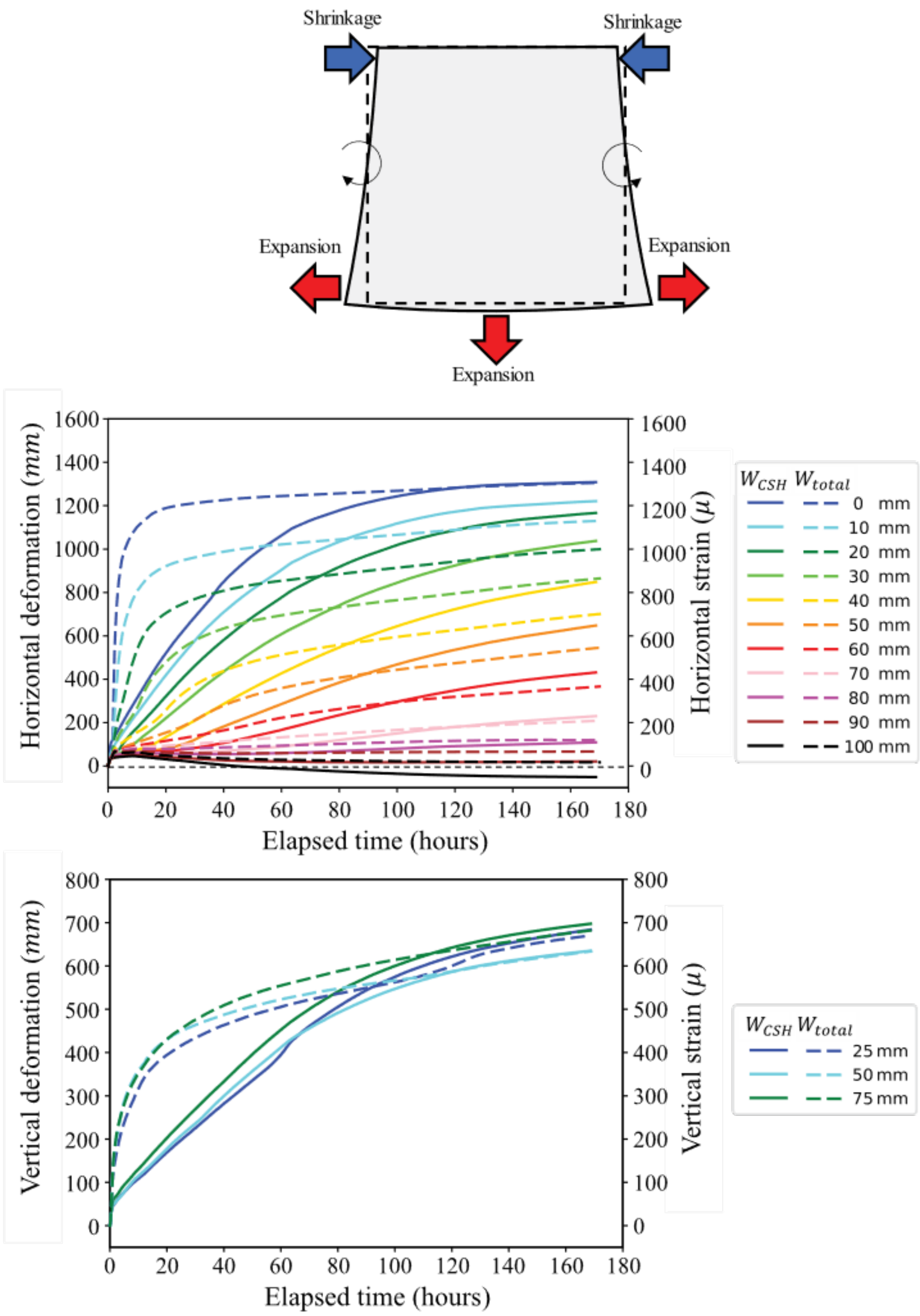

Fig. 15. Influence of microstructural change of cement paste on concrete expansion.

The numerical results reported the homogenous expansion occurred after the liquid water uptake was initiated and the shrinkage at the top of the specimen gradually developed along with the liquid water uptake progress. Although the aforementioned phenomenon was not measured by a strain gauge, the aforementioned homogenous expansion and shrinkage possibly occurred due to the compatibility of deformation. Under the free conditions, the sudden expansion of the bottom surface at the early period might induce the deformation of the entire body as observed in the maximum principal strain from the reference experiment (**Fig.** 9) and numerical study (**Fig.** 12). Whereas the shrinkage at the top of specimen occurred under the deformation compatibility regarding the bending deformation that increases with the expansion at the bottom of the specimen. Note that the homogenous expansion occurred for the cracked concrete only because it was not observed from the calculation of case C (without cracks).

Regarding the comparison of deformation (Fig. 15), it is worth mentioning that the MCCP-induced delayed expansion must be considered. This is to reproduce the realistic volumetric change of mortar that is the origin of microcracks and closure of cracks during the drying and rewetting process, respectively.

4.3 Expansion-induced closure of cracks during rewetting process

In the reference experiment, the expansion-induced closure of cracks was reported regarding the development and dissipation of principal strain at the initial sorption process. However, it is quite difficult to clarify the mechanism of cracks based on the DIC data. Owing to the validity of the proposed model, the mechanism was investigated by the numerical results.

Fig. 16 shows the stress distribution (vertical and horizontal direction) according to an uneven deformation between mortar and coarse aggregate. After the pre-drying process, the uneven shrinkage deformation of mortar caused the tensile stress in both horizontal and vertical directions, which induced microcracks perpendicular to the aggregate surface. During the rewetting process, the re-saturation of water induced the expansion of mortar causing the relief of tensile stress. At the first hour of the water uptake process, the tensile stress accumulated under the drying process decreased from the initial stage which is consistent with the expansive deformation (**Fig.** 15) and development of maximum principal strain over the entire specimen (**Fig.** 12) as described in the previous section. Due to the impact of the drying process, instead of returning to the initial stage, the reverse stress distribution was observed. The compressive stress regarding the mortar expansion induces the closure of cracks. A similar process was observed for the aggregate phase. The compressive stress, which developed from the pre-drying process, transformed into tensile stress under the compatibility of deformation. The tensile stress progressively developed along with the mortar expansion and formed expansive cracks, which are parallel to the aggregate surface. The mechanism is quite similar to cracking behavior according to the radiation-induced volumetric expansion of aggregate and mortar investigated by RBSM (Sasano et al., 2020).

Based on the numerical results, it is worth mentioning that the MCCP is the key phenomenon for the evaluation of structural performance and durability of concrete. Because microstructural change is the basis of various phenomena, the modeling of anomalous moisture transport in cracked concrete and mechanical responses must be considered as clarified in this study. Since we are focused on the concrete material at this stage, the impact on structural performance was not accentuated. However, we believe that the closure of existing cracks will cause an alteration in the structural performance of concrete structures. In addition, it should be noted this study accentuated the crack closure process under the free condition (only the internal restraint in concrete material). At the structure level, the impact of concrete expansion might be different because the external restraint and external force are dominant phenomena for the cracking behavior. Therefore, further investigations are required to clarify the impact on structural performance.

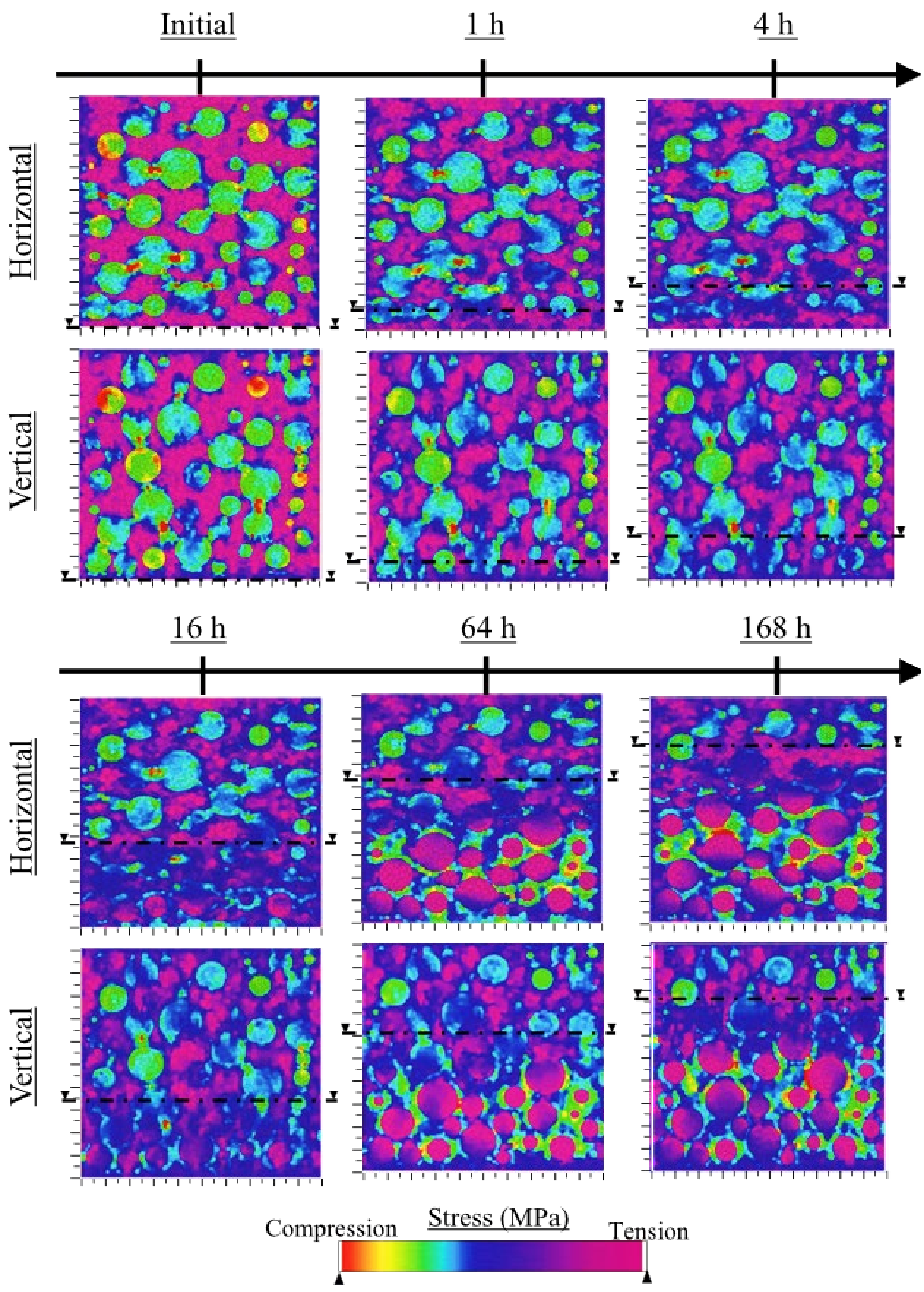

Fig. 16. Mechanism of expansion-induced closure of cracks during the rewetting process

5. Conclusions

This study aims to develop a mesoscale numerical method for evaluating moisture transport in cracked concrete. Because the moisture content in concrete is a key factor determining the deterioration of concrete, the quantitative evaluation of moisture transport is essential for clarifying the structural performance and durability of concrete structures. However, the anomalous behavior was reported according to the colloidal behavior of calcium-silicate-hydrate (C-S-H), which is a major component of cement paste, and the drying shrinkage-induced crack, which causes the rapid moisture transport into concrete and water redistribution from crack surfaces into the concrete matrix.

To reasonably reproduce the anomalous behavior, the colloidal behavior of C-S-H, and rapid absorption through cracks were reproduced based on the dynamic microstructural model, and Lucas-Washburn equation, respectively. The numerical investigation was conducted based on a reference experiment that investigated the liquid water uptake in oven-dried concrete based on the 2D-strain distribution from the digital image correlation (DIC) method. The good agreement of penetration depth development and mechanical responses obtained from numerical and experimental studies shows the validity of the proposed modeling approach for evaluating the liquid water uptake in cracked concrete. Owing to the validity of the modeling approach, further numerical investigation was conducted. The conclusions of the numerical investigation are summarized as follows.

1) Anomalous liquid water uptake is the consequence of both microstructural change of cement paste (MCCP) and drying shrinkage cracks, which affect the anomalous behavior at the later and initial stages, respectively.
2) Mortar expansion-induced closure of cracks was observed along with the liquid water uptake process, however, expansive cracks initiated around the aggregate surface
3) Volume change of mortar should be computed based on the microstructural change concept (corresponding to water content in interlayer spaces and gel pores) to reproduce the gradual expansion in accordance with the water redistribution in the C-S-H structure.
4) Closure of drying shrinkage cracks was induced by the development of compressive stress according to restrained mortar expansion, while expansive cracks were initiated regarding the tensile stress accumulated in the aggregate phase.
5) The alteration of cracks during the rewetting process indicated the impact of liquid water uptake on mechanical properties and durability of concrete. However, the impact on the structural level must be further investigated when external restraint and force are dominant for cracking behavior.

Acknowledgments

This research was supported by the JAEA Nuclear Energy S&T and Human Resource Development Project under Grant Number JPJA20P20333545.

References

Aldea, C.-M., Shah, S. P., & Karr, A. (1999). Effect of Cracking on Water and Chloride Permeability of Concrete. *Journal of Materials in Civil Engineering*, *11*(3). https://doi.org/10.1061/(asce)0899-1561(1999)11:3(181)

Alderete, N. M., Villagrán Zaccardi, Y. A., & De Belie, N. (2019). Physical evidence of swelling as the cause of anomalous capillary water uptake by cementitious materials. *Cement and Concrete Research*, *120*. https://doi.org/10.1016/j.cemconres.2019.04.001

Asselin, A., Charron, J. P., Desmettre, C., Benboudjema, F., & Oliver-Leblond, C. (2023). Numerical simulations for the determination of chloride diffusivity in reinforced concrete under tensile load. In *RILEM Bookseries* (Vol. 43). https://doi.org/10.1007/978-3-031-33211-1_42

Bolander, J. E., & Berton, S. (2004). Simulation of shrinkage induced cracking in cement composite overlays. *Cement and Concrete Composites*, *26*(7), 861–871. https://doi.org/10.1016/j.cemconcomp.2003.04.001

Bolander, J. E., & Saito, S. (1998). Fracture analyses using spring networks with random geometry. *Engineering Fracture Mechanics*, *61*(5–6), 569–591. https://doi.org/10.1016/S0013-7944(98)00069-1

De. Schutter, G. (1999). Quantification of the influence of cracks in concrete structures on carbonation and chloride penetration. *Magazine of Concrete Research*, *51*(6), 427–435. https://doi.org/10.1680/macr.1999.51.6.427

Diamond, S., & Huang, J. (2001). The ITZ in concrete - A different view based on image analysis and SEM observations. *Cement and Concrete Composites*, *23*(2–3). https://doi.org/10.1016/S0958-9465(00)00065-2

Fischer, N., Haerdtl, R., & McDonald, P. J. (2015). Observation of the redistribution of nanoscale water filled porosity in cement based materials during wetting. *Cement and Concrete Research*, *68*. https://doi.org/10.1016/j.cemconres.2014.10.013

Gajewicz, A. M., Gartner, E., Kang, K., McDonald, P. J., & Yermakou, V. (2016). A 1H NMR relaxometry investigation of gel-pore drying shrinkage in cement pastes. *Cement and Concrete Research*, *86*. https://doi.org/10.1016/j.cemconres.2016.04.013

Gardner, D., Jefferson, A., & Hoffman, A. (2012). Investigation of capillary flow in discrete cracks in cementitious materials. *Cement and Concrete Research*, *42*(7). https://doi.org/10.1016/j.cemconres.2012.03.017

Hall, C. (2007). Anomalous diffusion in unsaturated flow: Fact or fiction? In *Cement and Concrete Research* (Vol. 37, Issue 3). https://doi.org/10.1016/j.cemconres.2006.10.004

Hall, C., Hoff, W. D., Taylor, S. C., Wilson, M. A., Yoon, B. G., Reinhardt, H. W., Sosoro, M., Meredith, P., & Donald, A. M. (1995). Water anomaly in capillary liquid absorption by cement-based materials. *Journal of Materials Science Letters*, *14*(17), 1178–1181. https://doi.org/10.1007/BF00291799

Hamraoui, A., & Nylander, T. (2002). Analytical approach for the Lucas-Washburn equation. *Journal of Colloid and Interface Science*, *250*(2). https://doi.org/10.1006/jcis.2002.8288

Janota, M., Istok, O., Faux, D. A., & McDonald, P. J. (2022). Factors influencing the time dependence of porosity relaxation in cement during sorption: Experimental results from spatially resolved NMR. *Cement*, *8*. https://doi.org/10.1016/j.cement.2022.100028

Jebli, M., Jamin, F., Malachanne, E., Garcia-Diaz, E., & El Youssoufi, M. S. (2018). Experimental characterization of mechanical properties of the cement-aggregate interface in concrete. *Construction and Building Materials*, *161*. https://doi.org/10.1016/j.conbuildmat.2017.11.100

Jennings, H. M. (2000). Model for the microstructure of calcium silicate hydrate in cement paste. *Cement and Concrete Research*, *30*(1). https://doi.org/10.1016/S0008-8846(99)00209-4

Jennings, H. M. (2008). Refinements to colloid model of C-S-H in cement: CM-II. *Cement and Concrete Research*, *38*(3). https://doi.org/10.1016/j.cemconres.2007.10.006

Jennings, H. M., Bullard, J. W., Thomas, J. J., Andrade, J. E., Chen, J. J., & Scherer, G. W. (2008). Characterization and modeling of pores and surfaces in cement paste: Correlations to processing and properties. *Journal of Advanced Concrete Technology*, *6*(1). https://doi.org/10.3151/jact.6.5

Kawai, T. (1978). New discrete models and their application to seismic response analysis of structures. *Nuclear Engineering and Design*, *48*(1), 207–229. https://doi.org/10.1016/0029-5493(78)90217-0

Kiran, R., Samouh, H., Igarashi, G., Haji, T., Ohkubo, T., Tomita, S., & Maruyama, I. (2020). Temperature-dependent water redistribution from large pores to fine pores after water uptake in hardened cement paste. *Journal of Advanced Concrete Technology*, *18*(10), 588–599. https://doi.org/10.3151/jact.18.588

Kiran, R., Samouh, H., Matsuda, A., Igarashi, G., Tomita, S., Yamada, K., & Maruyama, I. (2021). Water uptake in OPC and FAC mortars under different temperature conditions. *Journal of Advanced Concrete Technology*, *19*(3), 168–180. https://doi.org/10.3151/jact.19.168

Lockington, D. A., & Parlange, J. Y. (2003). Anomalous water absorption in porous materials. *Journal of Physics D: Applied Physics*, *36*(6). https://doi.org/10.1088/0022-3727/36/6/320

Logan, D. L. (2007). *A First Course in the Finite Element Method: Heat Transfer and Mass Transport* (4th ed.). THOMSON.

Martys, N. S., & Ferraris, C. F. (1997). Capillary transport in mortars and concrete. *Cement and Concrete Research*, *27*(5), 747–760. https://doi.org/10.1016/S0008-8846(97)00052-5

Maruyama, I. (2016). Multi-scale review for possible mechanisms of natural frequency change of reinforced concrete structures under an ordinary drying condition. *Journal of Advanced Concrete Technology*, *14*(11), 691–705. https://doi.org/10.3151/jact.14.691

Maruyama, I. (2022). Impact of drying on concrete and concrete structures. *RILEM Technical Letters*, *7*. https://doi.org/10.21809/rilemtechlett.2022.154

Maruyama, I., Igarashi, G., & Kishi, N. (2011). Fundamental study on water transfer in portland cement paste. *Journal of Structural and Construction Engineering*, *76*(668). https://doi.org/10.3130/aijs.76.1737

Maruyama, I., Kameta, S., Suzuki, M., & Sato, R. (2006). Cracking of high strength concrete around deformed reinforcing bar due to shrinkage. *Proceedings of International RILEM-JCI Seminar on Concrete Durability and Service Life Planning, ConcreteLife'06 104-111, 2006*, 104–111.

Maruyama, I., Nishioka, Y., Igarashi, G., & Matsui, K. (2014). Microstructural and bulk property changes in hardened cement paste during the first drying process. *Cement and Concrete Research*, *58*. https://doi.org/10.1016/j.cemconres.2014.01.007

Maruyama, I., Ohkubo, T., Haji, T., & Kurihara, R. (2019). Dynamic microstructural evolution of hardened cement paste during first drying monitored by 1H NMR relaxometry. *Cement and Concrete Research*, *122*. https://doi.org/10.1016/j.cemconres.2019.04.017

Maruyama, I., & Sasano, H. (2014). Strain and crack distribution in concrete during drying. *Materials and Structures/Materiaux et Constructions*, *47*(3). https://doi.org/10.1617/s11527-013-0076-7

Maruyama, I., Sasano, H., Nishioka, Y., & Igarashi, G. (2014). Strength and Young's modulus change in concrete due to long-term drying and heating up to 90 °c. *Cement and Concrete Research*, *66*. https://doi.org/10.1016/j.cemconres.2014.07.016

McDonald, P. J., Istok, O., Janota, M., Gajewicz-Jaromin, A. M., & Faux, D. A. (2020). Sorption, anomalous water transport and dynamic porosity in cement paste: A spatially localised 1H NMR relaxation study and a proposed mechanism. *Cement and Concrete Research*, *133*, 106045. https://doi.org/10.1016/j.cemconres.2020.106045

Monteiro, P. J. M., & Andrade, W. P. (1987). Analysis of the rock-cement paste bond using probabilistic treatment of brittle strength. *Cement and Concrete Research*, *17*(6). https://doi.org/10.1016/0008-8846(87)90080-9

Nakamura, H., Srisoros, W., Yashiro, R., & Kunieda, M. (2006). Time-dependent structural analysis considering mass transfer to evaluate deterioration process of RC structures. *Journal of Advanced Concrete Technology*, *4*(1), 147–158. https://doi.org/10.3151/jact.4.147

Nakarai, K., Morito, S., Ehara, M., & Matsushita, S. (2016). Shear strength of reinforced concrete beams: Concrete volumetric change effects. *Journal of Advanced Concrete Technology*, *14*(5). https://doi.org/10.3151/jact.14.229

Ogawa, K., Igarashi, G., & Maruyama, I. (2023). Evaluation of drying shrinkage cracking behavior of concrete surface using digital image correlation method. *Annual Proceeding of Architecture Institute of Japan 2023*, 1143 (In Japanese).

Paul, A., Laurila, T., Vuorinen, V., & Divinski, S. (2014). Fick's Laws of Diffusion. In *Thermodynamics, Diffusion and the Kirkendall Effect in Solids* (pp. 115–139). Springer International Publishing. https://doi.org/10.1007/978-3-319-07461-0_3

Pihlajavaara, S. E. (1974). A review of some of the main results of a research on the ageing phenomena of concrete: Effect of moisture conditions on strength, shrinkage and creep of mature concrete. *Cement and Concrete Research*, *4*(5). https://doi.org/10.1016/0008-8846(74)90048-9

Rao, G. A., & Prasad, B. K. R. (2011). Influence of interface properties on fracture behaviour of concrete. *Sadhana - Academy Proceedings in Engineering Sciences*, *36*(2). https://doi.org/10.1007/s12046-011-0012-x

Rodriguez, O. G., & Hooton, R. D. (2003). Influence of cracks on chloride ingress into concrete. *ACI Materials Journal*, *100*(2), 120–126. https://doi.org/10.14359/12551

Rucker-Gramm, P., & Beddoe, R. E. (2010). Effect of moisture content of concrete on water uptake. *Cement and Concrete Research*, *40*(1). https://doi.org/10.1016/j.cemconres.2009.09.001

Saeidpour, M., & Wadsö, L. (2015). Evidence for anomalous water vapor sorption kinetics in cement based materials. *Cement and Concrete Research*, *70*. https://doi.org/10.1016/j.cemconres.2014.10.014

Saito, S., & Hikosaka, H. (1999). Numerical analysis of reinforced concrete structures using spring network model. *Journal of Materials, Concrete Structures and Pavements, JSCE*, *44*(627), 289–303. https://doi.org/10.2208/jscej.1999.627_289.

Sasano, H., & Maruyama, I. (2019). Numerical study on the shear failure behavior of RC beams subjected to drying. *Nuclear Engineering and Design*, *351*, 203–211. https://doi.org/10.1016/j.nucengdes.2019.06.003

Sasano, H., & Maruyama, I. (2021). Mechanism of drying-induced change in the physical properties of concrete: A mesoscale simulation study. *Cement and Concrete Research*, *143*. https://doi.org/10.1016/j.cemconres.2021.106401

Sasano, H., Maruyama, I., Nakamura, A., Yamamoto, Y., & Teshigawara, M. (2018). Impact of drying on structural performance of reinforced concrete shear walls. *Journal of Advanced Concrete Technology*, *16*(5), 210–232. https://doi.org/10.3151/jact.16.210

Sasano, H., Maruyama, I., Sawada, S., Ohkubo, T., Murakami, K., & Suzuki, K. (2020). Meso-Scale modelling of the mechanical properties of concrete affected by radiation-induced aggregate expansion. *Journal of Advanced Concrete Technology*, *18*(10). https://doi.org/10.3151/JACT.18.648

Sato, R., & Kawakane, H. (2008). A new concept for the early age shrinkage effect on diagonal cracking strength of reinforced HSC beams. *Journal of Advanced Concrete Technology*, *6*(1). https://doi.org/10.3151/jact.6.45

Satya, P., Asai, T., Teshigawara, M., Hibino, Y., & Maruyama, I. (2021). Impact of drying on structural performance of reinforced concrete beam with slab. *Materials*, *14*(8). https://doi.org/10.3390/ma14081887

Scrivener, K. L., Crumbie, A. K., & Laugesen, P. (2004). The interfacial transition zone (ITZ) between cement paste and aggregate in concrete. *Interface Science*, *12*(4). https://doi.org/10.1023/B:INTS.0000042339.92990.4c

Sereda, P. J., Feldman, R. F., & Swenson, E. G. (1966). Effect of sorbed water on some mechanical properties of hydrated Portland cement pastes and compacts. *Highway Research Board*, *90*.

Setzer, M. J. (2009). The solid-liquid gel-system of hardened cement paste. *Creep, Shrinkage and Durability Mechanics of Concrete and Concrete Structures - Proceedings of the 8th Int. Conference on Creep, Shrinkage and Durability Mechanics of Concrete and Concrete Structures*, *1*. https://doi.org/10.1201/9780203882955.ch28

Singla, A., Šavija, B., Sluys, L. J., & Romero Rodríguez, C. (2022). Modelling of capillary water absorption in sound and cracked concrete using a dual-lattice approach: Computational aspects. *Construction and Building Materials*, *320*. https://doi.org/10.1016/j.conbuildmat.2021.125826

Srimook, P., & Maruyama, I. (2023a). Modelling of Moisture Transport in Cracked Concrete by Using RBSM and TNM. In *RILEM Bookseries* (Vol. 43). https://doi.org/10.1007/978-3-031-33211-1_99

Srimook, P., & Maruyama, I. (2023b). Simulation of anomalous liquid water uptake in OPC mortar with dynamic microstructural change model. *Cement Science and Concrete Technology*, *76*(1). https://doi.org/10.14250/cement.76.349

Srimook, P., Yamada, K., Tomita, S., Igarashi, G., Aihara, H., Tojo, Y., & Maruyama, I. (2023). Evaluation of seismic performance of aged massive RC wall structure restrained by adjacent members using RBSM. *Nuclear Engineering and Design*, *414*, 112602. https://doi.org/https://doi.org/10.1016/j.nucengdes.2023.112602

Tanimura, M., Sato, R., & Hiramatsu, Y. (2007). Serviceability performance evaluation of RC flexural members improved by using low-shrinkage high-strength concrete. *Journal of Advanced Concrete Technology*, *5*(2). https://doi.org/10.3151/jact.5.149

Taylor, S. C., Hoff, W. D., Wilson, M. A., & Green, K. M. (1999). Anomalous water transport properties of Portland and blended cement-based materials. *Journal of Materials Science Letters*, *18*(23), 1925–1927. https://doi.org/10.1023/A:1006677014070

Thomas, J. J., & Jennings, H. M. (2006). A colloidal interpretation of chemical aging of the C-S-H gel and its effects on the properties of cement paste. *Cement and Concrete Research*, *36*(1). https://doi.org/10.1016/j.cemconres.2004.10.022

Van Belleghem, B., Montoya, R., Dewanckele, J., Van Den Steen, N., De Graeve, I., Deconinck, J., Cnudde, V., Van Tittelboom, K., & De Belie, N. (2016). Capillary water absorption in cracked and uncracked mortar - A comparison between experimental study and finite element analysis. *Construction and Building Materials*, *110*. https://doi.org/10.1016/j.conbuildmat.2016.02.027

Villagrán Zaccardi, Y. A., Alderete, N. M., & De Belie, N. (2017). Improved model for capillary absorption in cementitious materials: Progress over the fourth root of time. *Cement and Concrete Research*, *100*. https://doi.org/10.1016/j.cemconres.2017.07.003

Wang, K., Jansen, D. C., Shah, S. P., & Karr, A. F. (1997). Permeability study of cracked concrete. *Cement and Concrete Research*, *27*(3). https://doi.org/10.1016/S0008-8846(97)00031-8

Wang, L., Bao, J., & Ueda, T. (2016). Prediction of mass transport in cracked-unsaturated concrete by mesoscale lattice model. *Ocean Engineering*, *127*. https://doi.org/10.1016/j.oceaneng.2016.09.044

Washburn, E. W. (1921). The dynamics of capillary flow. *Physical Review*, *17*(3), 273–283.

Witherspoon, P. A., Wang, J. S. Y., Iwai, K., & Gale, J. E. (1980). Validity of Cubic Law for fluid flow in a deformable rock fracture. *Water Resources Research*, *16*(6). https://doi.org/10.1029/WR016i006p01016

Wittmann, F. (1968). Surface tension shrinkage and strength of hardened cement paste. *Matériaux et Construction*, *1*(6). https://doi.org/10.1007/BF02473643

Wu, Z., Wong, H. S., Chen, C., & Buenfeld, N. R. (2019). Anomalous water absorption in cement-based materials caused by drying shrinkage induced microcracks. *Cement and Concrete Research*, *115*. https://doi.org/10.1016/j.cemconres.2018.10.006

Xie, Y., Corr, D. J., Jin, F., Zhou, H., & Shah, S. P. (2015). Experimental study of the interfacial transition zone (ITZ) of model rock-filled concrete (RFC). *Cement and Concrete Composites*, *55*. https://doi.org/10.1016/j.cemconcomp.2014.09.002

Yamada, K., Takeuchi, Y., Igarashi, G., & Osako, M. (2019). Field survey of radioactive cesium contamination in concrete after the fukushima-daiichi nuclear power station accident. *Journal of Advanced Concrete Technology*, *17*(12). https://doi.org/10.3151/jact.17.659

Yamamoto, Y., Nakamura, H., Kuroda, I., & Furuya, N. (2008). Analysis of compression failure of concrete by three dimensional rigid body spring model. *Doboku Gakkai Ronbunshuu E*, *64*(4), 612-630. (In Japanese). https://doi.org/10.2208/jsceje.64.612

Yamamoto, Y., Nakamura, H., Kuroda, I., & Furuya, N. (2014). Crack propagation analysis of reinforced concrete wall under cyclic loading using RBSM. *European Journal of Environmental and Civil Engineering*, *18*(7), 780–792. https://doi.org/10.1080/19648189.2014.881755

Yang, Z., Weiss, W. J., & Olek, J. (2006). Water Transport in Concrete Damaged by Tensile Loading and Freeze–Thaw Cycling. *Journal of Materials in Civil Engineering*, *18*(3). https://doi.org/10.1061/(asce)0899-1561(2006)18:3(424)

Yurtdas, I., Burlion, N., & Shao, J. F. (2015). Evolution of mechanical behaviour of mortar with re-saturation after drying. *Materials and Structures/Materiaux et Constructions*, *48*(10).

https://doi.org/10.1617/s11527-014-0403-7

Yurtdas, I., Burlion, N., & Skoczylas, F. (2004a). Experimental characterisation of the drying effect on uniaxial mechanical behaviour of mortar. *Materials and Structures/Materiaux et Constructions*, *37*(267). https://doi.org/10.1617/13915

Yurtdas, I., Burlion, N., & Skoczylas, F. (2004b). Triaxial mechanical behaviour of mortar: Effects of drying. *Cement and Concrete Research*, *34*(7). https://doi.org/10.1016/j.cemconres.2003.12.004

Yurtdas, I., Peng, H., Burlion, N., & Skoczylas, F. (2006). Influences of water by cement ratio on mechanical properties of mortars submitted to drying. *Cement and Concrete Research*, *36*(7). https://doi.org/10.1016/j.cemconres.2005.12.015

Zhang, P., Wang, P., Hou, D., Liu, Z., Haist, M., & Zhao, T. (2017). Application of neutron radiography in observing and quantifying the time-dependent moisture distributions in multi-cracked cement-based composites. *Cement and Concrete Composites*, *78*. https://doi.org/10.1016/j.cemconcomp.2016.12.006

Zhang, P., Wittmann, F. H., Zhao, T., & Lehmann, E. (2010). Neutron imaging of water penetration into cracked steel reinforced concrete. *Physica B: Condensed Matter*, *405*(7). https://doi.org/10.1016/j.physb.2010.01.065

Zhang, Z., & Angst, U. (2020). A Dual-Permeability Approach to Study Anomalous Moisture Transport Properties of Cement-Based Materials. *Transport in Porous Media*, *135*(1). https://doi.org/10.1007/s11242-020-01469-y

Zhou, C., Ren, F., Wang, Z., Chen, W., & Wang, W. (2017). Why permeability to water is anomalously lower than that to many other fluids for cement-based material? *Cement and Concrete Research*, *100*. https://doi.org/10.1016/j.cemconres.2017.08.002

Zimbelmann, R. (1985). A contribution to the problem of cement-aggregate bond. *Cement and Concrete Research*, *15*(5). https://doi.org/10.1016/0008-8846(85)90146-2